Intrinsic Topological Superconductors with Triplet Pairing

Bachelor's Thesis

Clara Neerup Breiø

July 16, 2017

Supervisor
Brian Møller Andersen

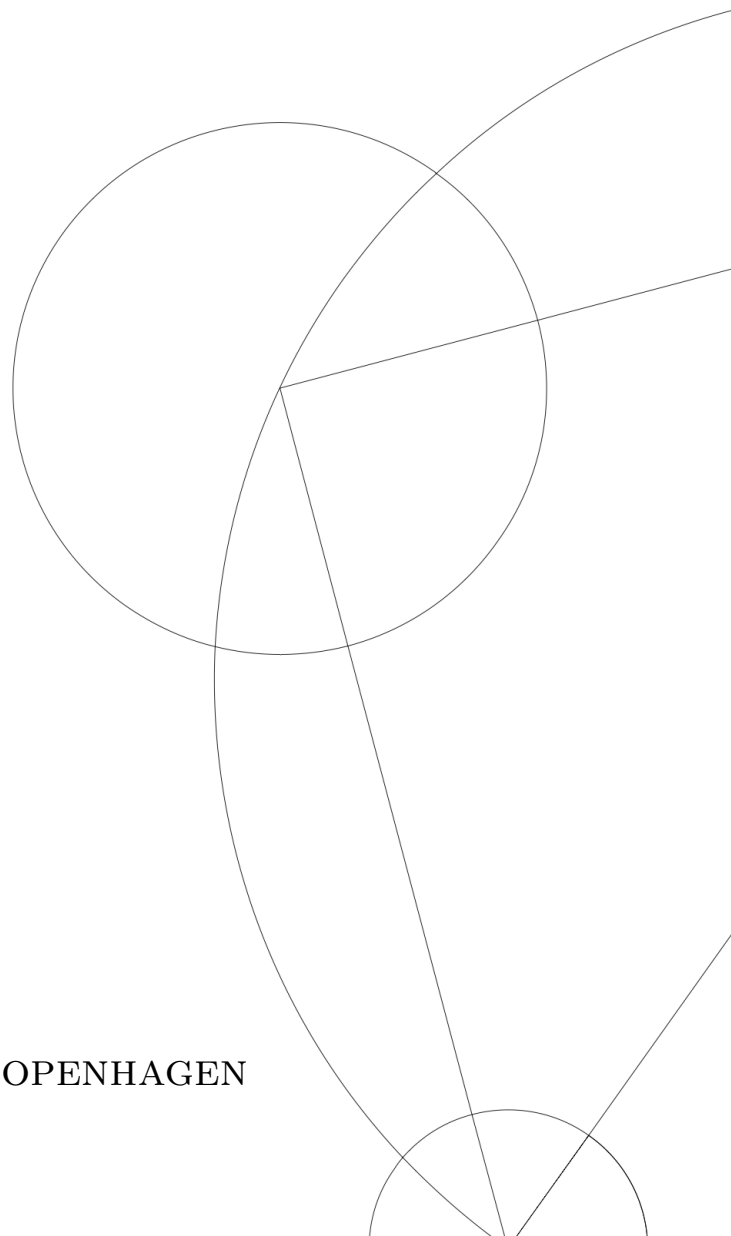

University of Copenhagen

UNIVERSITY OF
COPENHAGEN

Name of Institute:	Niels Bohr Institute
Name of Department:	Condensed Matter Theory
Author:	Clara Neerup Breiø
Email:	claranebr@gmail.com

Title and subtitle:	Intrinsic Topological Superconductors with Triplet Pairing
Supervisor:	Brian Møller Andersen
Handed in:	14.06.2017
Defended:	07.07.2017

Name _____

Signature _____

Date _____

Abstract

In this thesis, we investigate a $p_x + ip_y$ superconductor. This is an intrinsic topological superconductor subject to immense scientific interest, due to the possible hosting of Majorana fermions. We determine the Bogoliubov-de Gennes equation and discuss the chirality as well as the topology of the system. Subsequently we present results obtained from self-consistent numerical solutions to the Bogoliubov-de Gennes equation. We first study the case with open boundary conditions yielding chiral edge states. We further impose a vortex and confirm the guaranteed zero-energy excitation in the core. Finally we display results obtained from invoking a half-quantum vortex and argue that the zero-energy excitation in the core is a topologically protected Majorana zero mode.

Contents

1 Introduction

Over the past four decades the field of exotic superconductors has attracted immense scientific interest [1–3]. In particular the subclass of topological superconductors have proven to be suitable candidates for hosting the infamous Majorana zero modes [2]. A striking example of this is the layered Sr_2RuO_4 which exhibits chiral $p_x + ip_y$ superconductivity [2,4]. The likely existence of Majorana fermions in such intrinsic topological superconductors has led to the belief that a full understanding of these could be a crucial step towards the realization of a topological quantum computer [5]. Recent studies suggest half-quantum vortex cores to be one of the most promising hosts of Majorana zero modes in a spinful chiral p-wave superconductor [6].

In this thesis the exotic features of a $p_x + ip_y$ superconductor are investigated. A general introduction to superconductivity and Majorana fermions is given in Section 2. In Section 3 the relevant Hamiltonian is presented and the corresponding Bogoliubov-de Gennes equation and chirality is discussed, while Section 4 is a discussion of the model's topology. These three sections all prepare for the presentation of the numerical results in Section 5. We first present results yielding edge localized states in the case of a finite system followed by a discussion of regular vortices and the corresponding zero-energy excitations in the $p_x + ip_y$ superconductor. Finally we give an introduction to half-quantum vortices and present results obtained from implementing this exotic phenomenon.

2 Superconductivity

The field of low temperature physics took its first steps in the laboratory of H. Krammerling Onnes in 1908 with the liquefaction of ^{4}He followed by the discovery of superconducting Hg in 1911 [3]. With this the existence of a completely new class of materials, known as superconductors, had been uncovered. Superconductors are materials which, among other key properties, are characterized by zero resistivity and the expulsion of magnetic fields (known as the Meissner-Ochsenfeld effect) [3]. The journey towards a theoretical understanding of these effects took its first step in 1935, where the London brothers developed their theory based on the works by Drude and Maxwell. They reached a theoretical explanation of the Meissner-Ochsenfeld effect, but their theory did not cover anything near to a complete understanding of superconductivity.
The next big theoretical advance was done in the light of thermodynamic phase transitions. Landau had previously studied different phase transitions based on the principle of free energy minimization. In collaboration with Ginzburg he presented the Ginzburg-Landau (GL) model in 1950, which introduced a complex order parameter, $\psi(\mathbf{r})$, characterizing the superconducting state. Among other crucial predictions, their theory was able to provide a greater understanding of the flux quantization of type II superconductors [3]. Despite the many correct results obtained through the two macroscopic theories above, it was well-known that they did not provide the full microscopic picture.

2.1 BCS Theory[1]

Bardeen, Cooper and Schrieffer (BCS) thus set in all efforts to develop the first microscopic description of superconductivity. In their theory, published in 1957, the complex order parameter, $\psi(\mathbf{r})$, known from GL theory, was related to the superconducting order parameter Δ while $|\psi|^2$ was interpreted as the density of so-called Cooper pairs.
BCS theory relies on the rather astonishing result that at low temperatures the effective electron-electron interaction near the Fermi surface is attractive rather than repulsive. Since the full derivation of this conclusion is based on Feynman diagrams and many-body Green's functions it is beyond the scope of this thesis. We will simply state the most important physical aspects.
First and foremost in a metal we should not consider bare electrons but quasiparticles. These quasiparticles can be described as the excitations in solids consisting of a moving electron surrounded by an exchange correlation hole. This exchange correlation hole stems from the Pauli exclusion principle as well as the Coulomb interaction, since these prevent electrons from occupying the same point. Thus

[1]This section is based on theory and historical reviews from [3].

between quasiparticles the Coulomb force is substantially reduced by an effective screening.
Secondly the electrons interact via the exchange of a phonon. BCS found that this electron-phonon interaction [2] could be approximated by

$$V_{eff}(\omega) = |g_{eff}|^2 \frac{1}{\omega^2 - \omega_D^2},$$

with ω as the frequency of the interacting phonon, ω_D the Debye frequency, a characteristic phonon frequency of the system, and g_{eff} being an approximation to the original matrix element describing the scattering of the electron with the phonon [3]. In the low temperature regime where $|\omega| < \omega_D$, this can be further reduced to $V_{eff} = -|g_{eff}|^2$, that is an attractive potential. The related effective Hamiltonian of the electron-electron interaction is

$$H = -|g_{eff}|^2 \sum_{\mathbf{k},\tilde{\mathbf{k}},\mathbf{q},\sigma_1,\sigma_2} c^\dagger_{\mathbf{k}+\mathbf{q}\sigma_1} c^\dagger_{\tilde{\mathbf{k}}-\mathbf{q}\sigma_2} c_{\mathbf{k}\sigma_1} c_{\tilde{\mathbf{k}}\sigma_2},$$

where we introduced the fermionic creation ($c^\dagger_{\mathbf{k}+\mathbf{q}\sigma_1}$) and annihilation ($c_{\mathbf{k}\sigma_1}$) operators. We see that the Hamiltonian describes two electrons with momenta $\mathbf{k}$ and $\tilde{\mathbf{k}}$ getting annihilated, while two electrons with momenta $\mathbf{k}+\mathbf{q}$ and $\tilde{\mathbf{k}}-\mathbf{q}$ are created. Hence this is simply a momentum transfer between the two. The readers not familiar with second quantization are referred to Chapter 1 of [7]. Due to the low energy regime, we restrict the summation to wave vectors with energies within $\pm\hbar\omega_D$ of the Fermi surface.

2.1.1 Cooper Pairs

Having argued for an attractive potential between electrons near the Fermi surface, we move on to discuss the allowed states of such two electrons and the corresponding energy.
Consider a spherical Fermi surface at zero temperature, that is a filled Fermi sea. Now add two electrons to the system. Since all states below k_F are occupied, the two added electrons must be placed outside the Fermi surface. The two will constitute a two particle wave function, $\Psi(\mathbf{r}_1,\sigma_1,\mathbf{r}_2,\sigma_2) = e^{i\mathbf{KR}}\psi(\mathbf{r}_1-\mathbf{r}_2)\chi_{\sigma_1\sigma_2}$, where $\mathbf{K}$ and $\mathbf{R}$ are the center of mass momentum and position, respectively. To minimize the energy there is no center of mass motion, thus our two particle state is described solely by the spatial part, $\psi(\mathbf{r}_1-\mathbf{r}_2)$, and spin part, $\chi_{\sigma_1\sigma_2}$. Taking the spin to be singlet pairing for now, we must demand an even spatial part. Expanding this in terms of the Bloch waves (assumed to be plane waves [3]), we get

$$\psi(\mathbf{r}_1-\mathbf{r}_2) = \sum_{\mathbf{k}} \phi_{\mathbf{k}} e^{i\mathbf{k}(\mathbf{r}_1-\mathbf{r}_2)},$$

where $\phi_{\mathbf{k}}$ are undetermined expansion coefficients. The demand of an even function implies $\phi_{\mathbf{k}} = \phi_{-\mathbf{k}}$. Since $\chi_{\sigma_1\sigma_2} = 1/\sqrt{2}(|\uparrow\downarrow\rangle - |\downarrow\uparrow\rangle)$ the two particle wave function can be written as a sum of Slater determinants,

$$\Psi(\mathbf{r}_1,\sigma_1,\mathbf{r}_2,\sigma_2) = \sum_{\mathbf{k}} \phi_{\mathbf{k}} \begin{vmatrix} \psi_{\mathbf{k}\uparrow}(\mathbf{r}_1) & \psi_{\mathbf{k}\downarrow}(\mathbf{r}_2) \\ \psi_{-\mathbf{k}\uparrow}(\mathbf{r}_1) & \psi_{-\mathbf{k}\downarrow}(\mathbf{r}_2) \end{vmatrix} \Rightarrow |\Psi\rangle = \sum_{\mathbf{k}} \phi_{\mathbf{k}} |\Psi_{\mathbf{k}}\rangle ,$$

where $\psi_{\mathbf{k}}(\mathbf{r}) = e^{i\mathbf{kr}}$ and we imposed the condition that $\mathbf{k}_2 = -\mathbf{k}_1$ to minimize the energy. This wave function must obey the two particle Schrödinger equation

$$\sum_{\mathbf{k}} (\varepsilon_{\mathbf{k}} + \varepsilon_{-\mathbf{k}}) \phi_{\mathbf{k}} |\Psi_{\mathbf{k}}\rangle - |g_{eff}|^2 \sum_{\mathbf{k}} \phi_{\mathbf{k}} |\Psi_{\mathbf{k}}\rangle = E |\Psi\rangle . \tag{2.1}$$

The first term is nothing but the kinetic energy of the two pairs in the Slater determinant measured relative to ε_F, while the second term describes the effective electron-electron interaction. To obtain an

[2] The interaction is formally described as the vertex of the related Feynman diagram. The interested reader is referred to Chapter 17 of [7].

expression for the energy of the two particle state, we pick out the terms for a given $\mathbf{k}$ by multiplying Eq. 2.1 with $\langle\Psi_{\mathbf{k}}|$. Using that $\varepsilon_{\mathbf{k}} = \varepsilon_{-\mathbf{k}}$ and that $|g_{eff}|^2$ will ensure scattering from $(\mathbf{k}, -\mathbf{k})$ to $(\mathbf{k}', -\mathbf{k}')$, we find

$$
\begin{aligned}
2\varepsilon_{\mathbf{k}}\phi_{\mathbf{k}} - |g_{eff}|^2 \sum_{\mathbf{k}'} \phi_{\mathbf{k}'} &= E\phi_{\mathbf{k}}\,, \\
\phi_{\mathbf{k}} &= -\sum_{\mathbf{k}'} \phi_{\mathbf{k}'} |g_{eff}|^2 \frac{1}{E - 2\varepsilon_{\mathbf{k}}}\,, \\
\sum_{\mathbf{k}} \phi_{\mathbf{k}} &= -\sum_{\mathbf{k}'} \phi_{\mathbf{k}'} |g_{eff}|^2 \sum_{\mathbf{k}} \frac{1}{E - 2\varepsilon_{\mathbf{k}}}\,, \\
1 &= -|g_{eff}|^2 \sum_{\mathbf{k}} \frac{1}{E - 2\varepsilon_{\mathbf{k}}}\,, \\
1 &= -|g_{eff}|^2 \int_0^{\hbar\omega_D} \mathrm{d}\varepsilon g(\varepsilon) \frac{1}{E - 2\varepsilon}\,.
\end{aligned}
$$

In the last equality we used that a sum over $\mathbf{k}$ can always be converted into an integral over the density of states[3]. Furthermore we invoked the limits due to the restriction on the attractive potential as discussed previously. Given that the density of states is approximately constant within this small interval around the Fermi surface, this can be taken out of the integral, and we find

$$
1 = |g_{eff}|^2 g(0) \int_0^{\hbar\omega_D} \mathrm{d}\varepsilon \frac{1}{2\varepsilon - E} = \frac{|g_{eff}|^2 g(0)}{2} \ln\left(\frac{2\hbar\omega_D - E}{-E}\right).
$$

In the weak coupling limit, $|g_{eff}|^2 g(0) << 1$, this can be solved for E to yield,

$$
E = -2\hbar\omega_D e^{-2/|g_{eff}|^2 g(0)}\,. \tag{2.2}
$$

This result is rather astonishing, since it shows that the electron pair will form a bound state, that is with energy less that $2\varepsilon_F$, as soon as any attractive potential is present. Cooper thus reached the conclusion that the filled Fermi sea must be unstable against the formation of bound electron pairs known as Cooper pairs. E is the energy scale relevant when studying superconductors, which explains the very low critical temperature in conventional superconductors.

2.1.2 The Mean-Field Hamiltonian

With the formation of Cooper pairs in place, we wish to study the full system of a superconductor rather than the two particle wave function. To do so it is convenient to write up the effective Hamiltonian in terms of creation and annihilation operators,

$$
H = \sum_{\mathbf{k}\sigma} (\varepsilon_{\mathbf{k}} - \mu) c^\dagger_{\mathbf{k}\sigma} c_{\mathbf{k}\sigma} - |g_{eff}|^2 \sum_{\mathbf{k},\tilde{\mathbf{k}}} c^\dagger_{\mathbf{k}\uparrow} c^\dagger_{-\mathbf{k}\downarrow} c_{-\tilde{\mathbf{k}}\downarrow} c_{\tilde{\mathbf{k}}\uparrow}. \tag{2.3}
$$

We subtract the chemical potential to show explicitly that we set the zero kinetic energy at the Fermi surface. The ground state of this effective Hamiltonian is known as the BCS ground state, which is a product of the filled zero-temperature Fermi sea with 0,1,2,3 etc. Cooper pairs. The potential term of the Hamiltonian is quartic in the particle field operators and analytically unsolvable except in very limited 1D systems. Performing a mean-field decomposition allows us to rewrite it in a quadratic form,

$$
\begin{aligned}
H &= \sum_{\mathbf{k}\sigma} (\varepsilon_{\mathbf{k}} - \mu) c^\dagger_{\mathbf{k}\sigma} c_{\mathbf{k}\sigma} - |g_{eff}|^2 \sum_{\mathbf{k},\tilde{\mathbf{k}}} \left(c^\dagger_{\mathbf{k}\uparrow} c^\dagger_{-\mathbf{k}\downarrow} \langle c_{-\tilde{\mathbf{k}}\downarrow} c_{\tilde{\mathbf{k}}\uparrow} \rangle + \langle c^\dagger_{\mathbf{k}\uparrow} c^\dagger_{-\mathbf{k}\downarrow} \rangle c_{-\tilde{\mathbf{k}}\downarrow} c_{\tilde{\mathbf{k}}\uparrow} \right), \\
H &= \sum_{\mathbf{k}\sigma} (\varepsilon_{\mathbf{k}} - \mu) c^\dagger_{\mathbf{k}\sigma} c_{\mathbf{k}\sigma} - \sum_{\mathbf{k}} \left(\Delta c^\dagger_{\mathbf{k}\uparrow} c^\dagger_{-\mathbf{k}\downarrow} + h.c \right),
\end{aligned} \tag{2.4}
$$

[3]Never forget.

where we defined

$$\Delta \equiv |g_{eff}|^2 \sum_{\mathbf{k}} \langle c_{-\tilde{\mathbf{k}}\downarrow} c_{\tilde{\mathbf{k}}\uparrow} \rangle \,. \tag{2.5}$$

This is the previously mentioned superconducting order parameter (OP) replacing $\psi(\mathbf{r})$ from GL theory. Clearly $g_{eff} = 0$ corresponds to $\Delta = 0$ which emphasizes the fact that without an attractive potential, there is no superconductivity. Eq. 2.4 can be rewritten into matrix form as

$$H = \sum_{\mathbf{k}} \begin{pmatrix} c^\dagger_{\mathbf{k}\uparrow} & c_{-\mathbf{k}\downarrow} \end{pmatrix} \begin{pmatrix} \varepsilon_{\mathbf{k}} - \mu & -\Delta \\ -\Delta^* & -\varepsilon_{\mathbf{k}} + \mu \end{pmatrix} \begin{pmatrix} c_{\mathbf{k}\uparrow} \\ c^\dagger_{-\mathbf{k}\downarrow} \end{pmatrix} . \tag{2.6}$$

It is now straightforward to compute the eigenenergies of this Hamiltonian, which are

$$E_{\mathbf{k}} = \pm \sqrt{(\varepsilon_{\mathbf{k}} - \mu)^2 + |\Delta|^2} \,. \tag{2.7}$$

From this it is evident that the superconducting OP defines an energy gap around the Fermi surface within which there can be no excitations. Δ is therefore commonly referred to as the superconducting gap.
The eigenvectors of H must correspond to some linear combination of $c_{\mathbf{k}\uparrow}$ and $c^\dagger_{-\mathbf{k}\downarrow}$ denoted by $\gamma_{\mathbf{k}\uparrow}$, which is a so-called quasiparticle and will be discussed in greater detail throughout this thesis. For now it is sufficient to state that they are excitations of the BCS ground state and their energies are $E_{\mathbf{k}}$.

2.2 Types of Superconductivity

As the attentive reader might have dwelled upon, we have thus far only considered Cooper pairs with singlet pairing. In addition it turns out that since the electron-electron interaction is independent of $\mathbf{q}$ the potential in real space can be expressed as $V_{eff} = -|g_{eff}|^2 \delta(\mathbf{r}_1 - \mathbf{r}_2)$ [3]. This implies no internal angular momentum, since only then, it will be possible for the two electrons to occupy the same point in space. The solution thus relies on an s-wave pairing, $l = 0$, of the two. This singlet s-wave pairing is the most common type of conventional superconductors, however some materials do exhibit other types of attractive potentials allowing different types of pairings. To generalize the theory discussed above one should consider all possible spin combinations of the Cooper pair while still restricting to momenta $(\mathbf{k}, -\mathbf{k})$. Doing so, it is natural to express a general superconducting OP in terms of the triplet and singlet pairing as follows [3, 8],

$$\begin{aligned} \hat{\Delta} &= \begin{pmatrix} \Delta^{++} \Delta^{+-} \\ \Delta^{-+} \Delta^{--} \end{pmatrix} = i(\Delta_s(\mathbf{k}) I + \mathbf{d}(\mathbf{k}) \cdot \boldsymbol{\sigma}) \sigma_y \,, \\ \hat{\Delta} &= \begin{pmatrix} -d_x(\mathbf{k}) + i d_y(\mathbf{k}) & d_z(\mathbf{k}) + \Delta_s(\mathbf{k}) \\ d_z(\mathbf{k}) - \Delta_s(\mathbf{k}) & d_x(\mathbf{k}) + i d_y(\mathbf{k}) \end{pmatrix} , \end{aligned} \tag{2.8}$$

where $+\,(-)$ is spin up (down) and $\boldsymbol{\sigma}$ is the Pauli matrices. We have split up the superconducting OP into $\Delta_s = 1/2(\Delta^{+-} - \Delta^{-+})$, the singlet OP, and $\mathbf{d} = 1/2(\Delta^{--} - \Delta^{++}, -i(\Delta^{--} + \Delta^{++}), \Delta^{+-} + \Delta^{-+})$, the triplet OP. This thesis will focus on p-wave pairing, $l = 1$, with spin triplet pairing primarily of type $|\uparrow\downarrow\rangle + |\downarrow\uparrow\rangle$, that is an OP with $\Delta_s = d_x = d_y = 0$ and $d_z \neq 0$.
An interesting feature of many non-s-wave superconductors is the presence of nodes in the superconducting gap. These are essentially points or lines at the Fermi surface, where the gap closes. Consider the $\mathbf{k}$ dependence of the singlet and triplet OPs, which describes both the spin and orbital $\mathbf{k}$ dependence. The OPs can be said to pick a direction in spin space which is then multiplied by a function $f(\mathbf{k})$ representing the orbital part of the wave function [9]. This part can be expanded in the basis of spherical harmonics as [10]

$$f(\mathbf{k}) = \sum_{m=-l}^{l} a_{ml}(\mathbf{k}) Y_l^m(\hat{\mathbf{k}}) \,.$$

Relating the spherical harmonics to an assumed spherical Fermi surface and taking $l = 0$ as in the previous section, it becomes clear why an s-wave superconductor has a full gap (that is with no nodes), since Y_0^0 is perfectly spherical. In general $f(\mathbf{k})$ will of course exhibit various shapes.

Some examples of p-wave gaps can be seen in Fig. 1. The **a)** and **b)** cases both correspond to the spin pairing investigated in the thesis, but we see the important difference of point nodes in the k_x phase as opposed to a full gap in the $k_x + ik_y$ phase. The transition from the k_x phase to the $k_x + ik_y$ phase can be understood by considering the condensation energy, that is the energy gained by the system in transitioning to a superconducting phase. The condensation energy depends on $|\Delta(\mathbf{k})|^2$ averaged over the entire Fermi surface [8], hence nodes are in general not preferred by superconductivity. However the $k_x + ik_y$ phase is a chiral superconducting state, where the phase of the complex $\Delta_\mathbf{k}$ precesses $+2\pi$ as $\mathbf{k}$ follows a closed path around the k_z axis. This exotic behavior implies edge currents, which are of course energetically costly. Therefore the p-wave superconductor will prefer the k_x phase close to T_c to avoid edge currents but as the temperature decreases it will at some point be favorable for the system to create edge currents but in turn transition to a phase with a fully gaped Fermi surface.

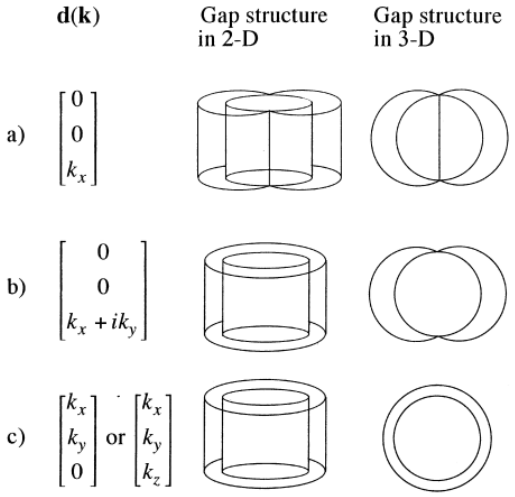

Figure 1: Examples of triplet OPs in a p-wave superconductor with their corresponding gap structure. The three cases correspond to three different superconducting phases. **a)** has point nodes in 2D and a line node in 3D, **b)** has a full gap in 2D and point nodes in 3D while **c)** has full gaps in both cases. This thesis will focus on case **b)** in 2D. The figure has been adopted from [9].

2.3 Majorana Fermions and Topological Superconductivity

A topological superconductor is a superconductor which exhibits symmetries such that a non-trivial topological invariant can be related to the system. Details of the topological classification and invariants will be discussed in Section 4. Let us for now simply state that the topological invariant determines the number of so-called Majorana fermions (MFs) in the system. MFs are a special type of quasiparticles represented by the previously mentioned $\gamma^\dagger$ operator. The MFs must satisfy the relation $\gamma = \gamma^\dagger$, that is they are their own hole. This requirement can be met by demanding equal electron and hole part. MFs are anyons, meaning that a particle exchange of two MFs can pick up any phase as opposed to usual fermions (always picking up -1). Furthermore they obey non-abelian statistics, implying that the exchange operations are non-commuting. Their non-abelian nature has led to the idea of low-decoherence topological quantum computation [5], and are thus of great scientific interest. In principle all fermionic operators can be written as a superposition of two Majorana operators as

$$c_i^\dagger = \frac{\gamma_{i,1} - \gamma_{i,2}}{2}, \tag{2.9}$$

in a real space representation, where $\gamma_{i,j}$ are MFs living on site i [5]. However these states are not topologically protected from decoherence and are of no significant importance. The term MF thus typically refers to a fermionic state with two spatially separated MFs. The most intuitive way to understand how such a state can appear, is to consider a 1D system with open the boundaries and an odd number of fermions located at individual sites represented by the blue boxes in Fig. 2 [4].

[4]This model is known as the Kitaev chain named after Alexei Kitaev who originally introduced it [11].

Figure 2: Illustration of the formation of delocalized fermionic states in a 1D system. The blue boxes correspond to fermion operators located at individual sites while the red dots correspond to Majorana operators. This figure has been adopted form [5].

According to Eq. 2.9 these can be split up into two Majorana operators represented by the red dots. If the topology is such that true MFs will appear, the Majorana operators will pair across neighboring sites to create fermions as depicted in the figure. The edge sites will thus create a highly delocalized fermionic state consisting of two true MFs, one at each edge. This delocalized fermionic state will not enter in the Hamiltonian written in terms of the operators creating/annihilating the pairs indicated by the dotted lines, and thus it must have zero energy cost [5]. Without any spatial overlap between the wave functions of the MFs they are protected from any local perturbation, since a such can only affect one of the two MFs constituting a pair.

3 The Bogoliubov-de Gennes Method

The previous section has been a discussion of some general phenomena necessary to form superconductivity or consequences thereof. In the remainder of this thesis we will investigate a particular superconducting system. The aim is to examine a $p_x + ip_y$ superconductor with triplet pairing of type $(|\uparrow\downarrow\rangle + |\downarrow\uparrow\rangle)/\sqrt{2}$ on a 2D square lattice.

The lattice Hamiltonian of a general superconducting system can be written,

$$H = -\sum_{i,j,\alpha} t_{ij} c^\dagger_{i,\alpha} c_{j,\alpha} - \mu \sum_{i,\alpha} c^\dagger_{i,\alpha} c_{i,\alpha} + V_{pair}, \tag{3.1}$$

where we applied the tight-binding model to a two-dimensional square lattice with sites $i = (i_x, i_y)$. $c^\dagger_{i,\alpha}$ ($c_{i,\alpha}$) is the creation (annihilation) operator, α is the spin, t_{ij} represents the kinetic energy related to hopping between sites, μ is the chemical potential and V_{pair} is the pairing interaction. V_{pair} is determined by an orbital part and a spin part. Assuming only one dominating orbital of the superconducting properties [12], we will solely consider the spin part. Decomposing this into singlet and triplet parts as discussed in Section 2.2, the potential can be written [12]

$$V_{pair} = \frac{1}{2} \sum_{i,j,\alpha_1 \sim \alpha_4} \sum_{m=0}^{3} g_{m,ji} (\sigma_m i\sigma_2)^\dagger_{\alpha_3\alpha_1} (\sigma_m i\sigma_2)_{\alpha_2\alpha_4} (c_{i\alpha_1} c_{j\alpha_3})^\dagger c_{i\alpha_2} c_{j\alpha_4}, \tag{3.2}$$

with $g_{0,ji}$ being the singlet component and $g_{1,ji}$, $g_{2,ji}$, $g_{3,ji}$ being the three triplet components. $\sigma_{1\sim3}$ are the Pauli matrices and σ_0 is the 2-by-2 identity matrix, while $\alpha_{1\sim4}$ are the spin indices and thus represent all possible combinations of the spin pairing of two electrons at different sites.

To simplify Eq. 3.2 the first step is to perform a mean-field decomposition similar to Eq. 2.4 yielding

$$V_{pair} = \frac{1}{2} \sum_{i,j,\alpha_1 \sim \alpha_4} \sum_{m=0}^{3} g_{m,ji} (\sigma_m i\sigma_2)^\dagger_{\alpha_3\alpha_1} (\sigma_m i\sigma_2)_{\alpha_2\alpha_4} \left(\langle c^\dagger_{j\alpha_3} c^\dagger_{i\alpha_1} \rangle c_{i\alpha_2} c_{j\alpha_4} + c^\dagger_{j\alpha_3} c^\dagger_{i\alpha_1} \langle c_{i\alpha_2} c_{j\alpha_4} \rangle \right).$$

Defining the superconducting and triplet OPs as follows,

$$\Delta_{ji,\alpha_2\alpha_4} = \sum_{m=0}^{3} d_{m,ji}(\sigma_m i\sigma_2)_{\alpha_2\alpha_4} \tag{3.3a}$$

$$d_{m,ji} = g_{m,ji} \sum_{\alpha_1\alpha_3} (\sigma_m i\sigma_2)^{\dagger}_{\alpha_3\alpha_1} \langle c_{i\alpha_1} c_{j\alpha_3} \rangle \,, \tag{3.3b}$$

$$\tag{3.3c}$$

enables us to write the full Hamiltonian as

$$H = -\sum_{i,j,\alpha} t_{ij} c^{\dagger}_{i,\alpha} c_{j,\alpha} - \mu \sum_{i,\alpha} c^{\dagger}_{i,\alpha} c_{i,\alpha} + \frac{1}{2} \sum_{i,j} \sum_{\alpha_2\alpha_4} \left(\Delta_{ji,\alpha_2\alpha_4} c^{\dagger}_{j\alpha_4} c^{\dagger}_{i\alpha_2} + h.c. \right) .$$

As mentioned previously our focus will be on the triplet pairing of type $(|\uparrow\downarrow\rangle + |\downarrow\uparrow\rangle)/\sqrt{2}$ corresponding to $d_{0,ji} = d_{1,ji} = d_{2,ji} = 0$ and $d_{3,ji} = d_{ji}$. To ensure this we set $g_{0_ji} = g_{1,ji} = g_{2,ji} = 0$ and $g_{3,ji} = g$. Having defined these values the terms left to consider is,

$$\Delta_{ji,\alpha_2\alpha_4} = d_{ji} \begin{pmatrix} 0 & 1 \\ 1 & 0 \end{pmatrix}_{\alpha_2\alpha_4} \tag{3.4a}$$

$$d_{ji} = g \left(\langle c_{i\uparrow} c_{j\downarrow} \rangle + \langle c_{i\downarrow} c_{j\uparrow} \rangle \right) . \tag{3.4b}$$

Note that d_{ji}, hence $\Delta_{ji,\alpha_2\alpha_4}$, is antisymmetric due to the fermionic nature of the operators. This suggests a further simplification to the Hamiltonian, since the spin summation can be performed yielding

$$\begin{aligned} H &= -\sum_{i,j,\alpha} t_{ij} c^{\dagger}_{i,\alpha} c_{j,\alpha} - \mu \sum_{i,\alpha} c^{\dagger}_{i,\alpha} c_{i,\alpha} + \frac{1}{2} \sum_{i,j} \left(d_{ji} \left(c^{\dagger}_{j\sigma} c^{\dagger}_{i-\sigma} + c^{\dagger}_{j-\sigma} c^{\dagger}_{i\sigma} \right) + h.c. \right) , \\ H &= \underbrace{-\sum_{i,j,\alpha} t_{ij} c^{\dagger}_{i,\alpha} c_{j,\alpha} - \mu \sum_{i,\alpha} c^{\dagger}_{i,\alpha} c_{i,\alpha}}_{H^0} + \underbrace{\sum_{i,j} \left(d_{ji} c^{\dagger}_{j\sigma} c^{\dagger}_{i-\sigma} + h.c. \right)}_{H^{\Delta}}, \end{aligned} \tag{3.5}$$

where the last term has been rewritten using the anticommutator relation of the operators, the antisymmetry of d_{ji} and exchanging the dummy indices. This effective Hamiltonian is quadratic in the creation (annihilation) operators and can be solved numerically without extensive complexity.

3.1 The Bogoliubov-de Gennes Equation

A common method of solving the real-space Hamiltonian (3.5) is by using the Bogoliubov-de Gennes (BdG) equation. The derivation of this equation relies on performing an appropriate Bogoliubov transformation which diagonalizes the Hamiltonian in the basis of a set of quasiparticle operators $(\gamma^{\dagger}_{\varepsilon}, \gamma_{\varepsilon})$. In our case, a suitable transformation reads,

$$\begin{pmatrix} c_{p\sigma} \\ c^{\dagger}_{p-\sigma} \end{pmatrix} = \sum_{\varepsilon>0} \begin{pmatrix} u_{p\epsilon\sigma} & v^{*}_{p\epsilon\sigma} \\ v_{p\epsilon-\sigma} & u^{*}_{p\epsilon-\sigma} \end{pmatrix} \begin{pmatrix} \gamma_{\epsilon\sigma} \\ \gamma^{\dagger}_{\epsilon-\sigma} \end{pmatrix}, \tag{3.6}$$

where the transformation matrix is unitary, thus $|u|^2 + |v|^2 = 1$. The summation over ε is chosen to cover half the eigenstates, since the transformation itself should not introduce twice the number of states in the system. The proceeding derivation is concerned with the computation of commutator relations and can be found in Appendix A. The BdG equation with the assumptions of Eq. 3.4 applied is,

$$E_{\varepsilon} \begin{pmatrix} u_{j\varepsilon\sigma} \\ v_{j\varepsilon-\sigma} \end{pmatrix} = \sum_{i} \begin{pmatrix} K_{ji} & d_{ji} \\ -d^{\dagger}_{ji} & -K^{*}_{ji} \end{pmatrix} \begin{pmatrix} u_{i\varepsilon\sigma} \\ v_{i\varepsilon-\sigma} \end{pmatrix}, \tag{3.7}$$

where $K_{ji} = -t_{ji} - \mu\delta_{ji}$. The spin index on the energies has been dropped, since they are spin degenerate. It is evident that the BdG equation is an eigenvalue problem and can be solved to find the excitation energies and wave functions of the quasiparticles.

3.2 Self-Consistency Condition of the d-vector

Eqs. 3.4b and 3.7 clearly constitute a self-consistent problem, since the expectation values of the operators will naturally depend on the eigenvectors of the BdG equation. Thus we wish to determine the self-consistent condition in terms of u and v. Rewriting the expectation values to the γ-basis yields,

$$\begin{aligned}\langle c_{i\uparrow}c_{j\downarrow}\rangle &= \Big\langle \sum_{\varepsilon}\Big(u_{i\varepsilon\uparrow}\gamma_{\varepsilon\uparrow} + v^*_{i\varepsilon\uparrow}\gamma^\dagger_{\varepsilon\downarrow}\Big)\Big(u_{j\varepsilon\downarrow}\gamma_{\varepsilon\downarrow} + v^*_{j\varepsilon\downarrow}\gamma^\dagger_{\varepsilon\uparrow}\Big)\Big\rangle \\ &= \sum_{\varepsilon}\Big(u_{i\varepsilon\uparrow}u_{j\varepsilon\downarrow}\langle\gamma_{\varepsilon\uparrow}\gamma_{\varepsilon\downarrow}\rangle + u_{i\varepsilon\uparrow}v^*_{j\varepsilon\downarrow}\langle\gamma_{\varepsilon\uparrow}\gamma^\dagger_{\varepsilon\uparrow}\rangle + v^*_{i\varepsilon\uparrow}u_{j\varepsilon\downarrow}\langle\gamma^\dagger_{\varepsilon\downarrow}\gamma_{\varepsilon\downarrow}\rangle + v^*_{i\varepsilon\uparrow}v^*_{j\varepsilon\downarrow}\langle\gamma^\dagger_{\varepsilon\downarrow}\gamma^\dagger_{\varepsilon\uparrow}\rangle\Big) \\ &= \sum_{\varepsilon}\Big(u_{i\varepsilon\uparrow}v^*_{j\varepsilon\downarrow}\langle\gamma_{\varepsilon\uparrow}\gamma^\dagger_{\varepsilon\uparrow}\rangle + v^*_{i\varepsilon\uparrow}u_{j\varepsilon\downarrow}\langle\gamma^\dagger_{\varepsilon\downarrow}\gamma_{\varepsilon\downarrow}\rangle\Big),\end{aligned}$$

where the last equality is simply obtained by using that the BSC ground state is not an eigenstate of the $\gamma^\dagger\gamma^\dagger$ or $\gamma\gamma$ operator. The expectation value of the occupation number operator, $\langle\gamma^\dagger_{\varepsilon\downarrow}\gamma_{\varepsilon\downarrow}\rangle$, is given by the Fermi-Dirac distribution, since the γ operators refer to fermionic excitations. Furthermore the quasiparticle energy is measured with respect to ε_F, hence $1 - f(E_\varepsilon) = f(-E_\varepsilon)$. We thus find

$$\langle c_{i\uparrow}c_{j\downarrow}\rangle = \sum_{\varepsilon}\left(u_{i\varepsilon\uparrow}v^*_{j\varepsilon\downarrow}f(-E_\varepsilon) + v^*_{i\varepsilon\uparrow}u_{j\varepsilon\downarrow}f(E_\varepsilon)\right).$$

To rewrite this expression it is useful to consider symmetries of the BdG equation (3.7) which has so far been written in the eigensystem $\left\{E_\varepsilon, \begin{pmatrix} u_{j\varepsilon\sigma} \\ v_{j\varepsilon-\sigma}\end{pmatrix}\right\}$. However identical equations are can be derived, if the eigensystem is shifted to $\left\{-E_\varepsilon, \begin{pmatrix} v^*_{j\varepsilon\sigma} \\ u^*_{j\varepsilon-\sigma}\end{pmatrix}\right\}$. Performing this shift to the last term yields,

$$\begin{aligned}\langle c_{i\uparrow}c_{j\downarrow}\rangle &= \sum_{\varepsilon}\left(u_{i\varepsilon\uparrow}v^*_{j\varepsilon\downarrow}f(-E_\varepsilon) + u_{i\varepsilon\uparrow}v^*_{j\varepsilon\downarrow}f(-E_\varepsilon)\right) \\ &= 2\sum_{\varepsilon}u_{i\varepsilon\uparrow}v^*_{j\varepsilon\downarrow}f(-E_\varepsilon) \\ &= \sum_{all\ \varepsilon}u_{i\varepsilon\uparrow}v^*_{j\varepsilon\downarrow}f(-E_\varepsilon).\end{aligned}$$

In the last line we remind ourselves of the implicit restriction to positive ε introduced in the definition of the Bogoliubov transformation (3.6), which is now expanded to include all values of ε. Similarly we obtain

$$\langle c_{i\downarrow}c_{j\uparrow}\rangle = \sum_{\varepsilon}v^*_{i\varepsilon\downarrow}u_{j\varepsilon\uparrow}f(E_\varepsilon).$$

We now have the condition,

$$d_{ji} = g\sum_{\varepsilon}\left(u_{i\varepsilon\uparrow}v^*_{j\varepsilon\downarrow}f(-E_\varepsilon) + v^*_{i\varepsilon\downarrow}u_{j\varepsilon\uparrow}f(E_\varepsilon)\right), \tag{3.8}$$

which allows us to solve Eq. 3.7 in a proper, self-consistent manner.

3.3 Chirality and Excitation Energies in k-space

So far the triplet pairing has been imposed on the system. It remains, however, to investigate the chirality of the system, which, as previously mentioned, is determined by the phase of the superconducting OP in **k**-space. To do so we perform a Fourier transform (FT) of Eq. 3.5 where we neglect all other interactions than nearest neighbor (NN) and set $t_{ji} = t$. The full transformation can be found in Appendix B, here we merely state the result

$$H = \sum_{\mathbf{k}}\begin{pmatrix} c^\dagger_{\mathbf{k}\sigma} & c_{-\mathbf{k}-\sigma}\end{pmatrix}\begin{pmatrix} \varepsilon_{\mathbf{k}} - \mu & d_{\mathbf{k}} \\ d^*_{\mathbf{k}} & -(\varepsilon_{\mathbf{k}} - \mu)\end{pmatrix}\begin{pmatrix} c_{\mathbf{k}\sigma} \\ c^\dagger_{-\mathbf{k}-\sigma}\end{pmatrix}, \tag{3.9}$$

where $\varepsilon_{\mathbf{k}} = -2t(\cos(k_x) + \cos(k_y))$ and $d_{\mathbf{k}} = 2d\,(\sin(k_x) + i\sin(k_y))$. The corresponding excitation energies are

$$E_{\mathbf{k}} = \pm\sqrt{(\varepsilon_{\mathbf{k}} - \mu)^2 + |d_{\mathbf{k}}|^2}. \tag{3.10}$$

These can be used to confirm the numerical result obtained when solving the BdG equation (3.7) using the quantization of $\mathbf{k}$ $(k_x, k_y = 0, \pm\frac{2\pi}{L}, \pm\frac{4\pi}{L}, ...)$.

The result in Eq. 3.9 naturally depends on the definition of the superconducting NN interaction. The specific expression of $d_{\mathbf{k}}$ is obtained by imposing the following interactions

$$d_{ji} = \begin{cases} -id & , \text{ for } i = j + \hat{x} \\ id & , \text{ for } i = j - \hat{x} \\ d & , \text{ for } i = j + \hat{y} \\ -d & , \text{ for } i = j - \hat{y} \\ 0 & , \text{ otherwise.} \end{cases} \tag{3.11}$$

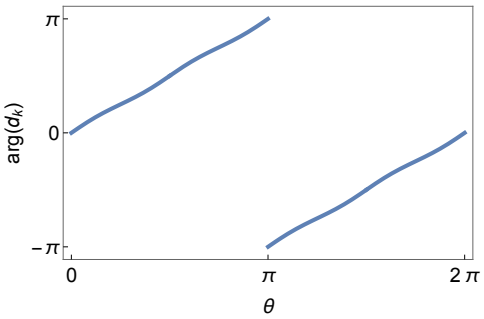

Figure 3: Phase of $d_{\mathbf{k}}$ as we precess $+2\pi$ around the z-axis. The plot confirms a winding of $+1$.

To determine the chirality, we express (k_x, k_y) as $(\cos(\theta), \sin(\theta))$ and plot the argument of $d_{\mathbf{k}}$ as a function of θ [5]. This yields the result shown in Fig. 3. Clearly the argument returns to its original value as we presses once around the z-axis, corresponding to a winding of $+1$ $(\times 2\pi)$.

With the BdG equation, self-consistency of $\mathbf{d}$ and desired chirality in place, we have a full, solvable description of a chiral p-wave superconductor of type $p_x + ip_y$.

3.4 Numerical Solution to the BdG Equation

Let us now discuss how to obtain the numerical solution to the BdG equation (3.7). The idea is to create an $N \times N$ square grid and enumerate each grid site. We do this by starting in one corner of the grid and scan upwards through all sites in vertical lines. Each site will correspond to both $u_{i\varepsilon\sigma}$ and $v_{i\varepsilon\sigma}$ values according to Eq. 3.7, hence the eigenvectors will have the form

$$\begin{pmatrix} u_{i\varepsilon\sigma} \\ v_{i\varepsilon\sigma} \end{pmatrix} \rightarrow \begin{pmatrix} u(1) \\ \cdot \\ \cdot \\ u(N^2) \\ v(1) \\ \cdot \\ \cdot \\ v(N^2) \end{pmatrix}$$

This leads to a BdG-matrix of dimensions $2N^2 \times 2N^2$ divided into four squares as follows

$$\left(\begin{array}{c|c} K_{ji} & d_{ji} \\ \hline -d_{ji}^{\dagger} & -K_{ji}^{*} \end{array}\right),$$

each square with N^2 entries. The on-site energy and NN hopping and coupling can be imposed by setting all other entries than these to zero. As an example take $u(5)$ in a 4×4 grid. With periodic

[5] Since the winding should be evaluated along the Fermi surface, we implicitly set $k_F = 1$. This is without any loss of generality, since the argument winding only changes by the enclosure of gap closings. In our case, the only gap closing within the Brillouin zone is at (0,0), the rest is situated at the edges. Thus the conclusion remains a winding of $+1$ as long as the Fermi surface has an approximately circular appearance.

boundary conditions, this site, 5, interacts with sites 1, 5, 6, 8 and 9. In the first square, K_{ji}, we set entry (5,5) to $-\mu$ and entries (5,1), (5,6), (5,8) and (5,9) to $-t$. Moving on to the superconducting couplings these combine $u(j)$ with $v(i)$ and vise versa, thus the NN entries of the second square will be (5,17), (5,22), (5,24) and (5,25). Now to ensure chiral p-wave superconductivity of type $p_x + ip_y$ we set the entries according to Eq. 3.11. Once the matrix is set up for all u and v and proper initial values for t, μ and d are chosen, the eigenvalues and vectors are computed and these values are used to set up a $\hat{d_{ji}}$-matrix applying Eq. 3.8, with each entry corresponding to a coupling between sites j and i. The new values for the couplings are inserted the BdG-matrix, and once again the eigenvectors and values are computed. The iterations continue until the error between the order parameters of two successive iterations falls below some predefined value. In practice the convergence condition used for the presented results is $|d(2N+4,2N+5)(n-1) - d(2N+4,2N+5)(n)| + |d(3N+5,2N+5)(n-1) - d(3N+5,2N+5)(n)| < 10^{-4}$ with n indicating the iteration number. The first term is a coupling in the x-direction and the second is a coupling in the y-direction, both between non-edge sites. This condition was chosen to ensure convergence of the interaction along both x and y, which is particularly relevant if we wish to study different boundary conditions in the two directions.

3.4.1 The Pairing Potential and Local Density of States

The excitation energies alone do not provide information regarding the localization of the excited quasiparticle states. As described in Section 2.3 the spatial separation of quasiparticles is essential to the formation of true MFs, thus we should not inspect the excitation energy spectrum itself but rather investigate the pairing potential (PP) and the local density of states (LDOS), which reveal the spatial extent of the excited states.
The PP at each site is

$$\Delta(\mathbf{r}_j) = \Delta_{p_x} + i\Delta_{p_y}, \tag{3.12}$$

with

$$\Delta_{p_x} = \frac{d_{j,j+\hat{x}} - d_{j,j-\hat{x}}}{2},$$
$$\Delta_{p_y} = \frac{d_{j,j+\hat{y}} - d_{j,j-\hat{y}}}{2}.$$

We see that the PP averages the intersite interaction at each site. A low potential will, not surprisingly, correspond to the quasiparticles preferred areas of inhabitance. This assertion is confirmed by inspecting the LDOS at zero energy. The general expression is given by [12],

$$LDOS(\mathbf{r}_j, \omega) = \sum_{\varepsilon} \left(|u_\varepsilon(\mathbf{r}_j)|^2 \delta(\omega - E_\varepsilon) + |v_\varepsilon(\mathbf{r}_j)|^2 \delta(\omega + E_\varepsilon) \right), \tag{3.13}$$

where ω denotes the entire energy spectrum. The derivation of the LDOS is beyond the scope of this thesis, however it is apparent that if a state is excited at energy E_1 the LDOS will have one spike at E_1 weighted by the amplitude of the creation (electron) operator and one spike at $-E_1$ weighted by the amplitude of the annihilation (hole) operator, which does indeed seem physically reasonable.
In the numerical computations the delta functions will be approximated by Lorentzians, that is $\delta(\omega \pm E_\varepsilon) \simeq -(1/\pi) Im((\omega \pm E_\varepsilon + i\eta)^{-1})$ with $\eta = 0.01t$.

The topological features of the superconductor will now be discussed and the results will be presented subsequently.

4 Symmetries and Topological Classification

Considering the symmetries and topological classification of our system is of the utmost relevance to perform a correct analysis of our results, since, as described in Section 2.3, the value of the topological invariant determines the number of possible Majorana modes in the system. To determine the topological properties of a system one should consider the non-simplified Hamiltonian. To do so we

	Symmetry	Condition	Unitarity
$\widehat{\Theta}$	Generalized time-reversal	$[\widehat{H}, \widehat{\Theta}] = 0$	Anti-unitary
$\widehat{\Xi}$	Charge-conjugation	$\{\widehat{H}, \widehat{\Xi}\} = 0$	Anti-unitary
$\widehat{\Pi}$	Chiral	$\{\widehat{H}, \widehat{\Pi}\} = 0$	Unitary

Table 1: The three operators to consider when topologically classifying a Hamiltonian. They each represent a symmetry which is present, if the corresponding condition is satisfied. The value of the operators' squares categorize systems into the ten symmetry classes in Table 2.

expand Eq. 3.9 to be written in terms of the four Nambu spinor $\Psi_{\mathbf{k}}^\dagger = \left(c_{\mathbf{k}\uparrow}^\dagger, c_{\mathbf{k}\downarrow}^\dagger, c_{-\mathbf{k}\downarrow}, -c_{-\mathbf{k}\uparrow}\right)$ and find

$$H = \frac{1}{2}\sum_{\mathbf{k}} \Psi_{\mathbf{k}}^\dagger \left[(\varepsilon_{\mathbf{k}} - \mu)\tau_z + 2d(\sin(k_x)\tau_x\sigma_z - \sin(k_y)\tau_y\sigma_z)\right]\Psi_{\mathbf{k}}\,, \tag{4.1}$$

where $\tau_{x,y,z}$ ($\sigma_{x,y,z}$) are the Pauli matrices referring to particle-hole space (spin space) and the factor of $1/2$ makes up for the double counting. We have omitted all the $\otimes$ in the tensor products as well as σ_I, the 2-by-2 identity matrix, in the first term. This is the full Fourier transform of Eq. 3.1 with the restrictions of Eq. 3.4 still applied. We now wish to block diagonalize Eq. 4.1 to simplify the further considerations. This can be done without any loss of generality by exchanging $c_{\mathbf{k}\downarrow}^\dagger$ and $c_{-\mathbf{k}\downarrow}$ in the Nambu spinor, yielding

$$H_\sigma = (\varepsilon_{\mathbf{k}} - \mu)\tau_z + \sigma 2d(\sin(k_x)\tau_x - \sin(k_y)\tau_y)\,, \tag{4.2}$$

with σ denoting the pseudospin, that is $\sigma = +1$ in the top block and $\sigma = -1$ in the bottom one. To classify the Hamiltonian in Eq. 4.2 we consider the three operators in Table 1 each representing a symmetry [13]. The symmetry represented by the given operator is present if it either commutes or anti-commutes (depending on the operator in question) with the Hamiltonian as expressed in the table. If that is indeed the case, the value of the operators' square determines the class of the system. Since $\widehat{\Theta}$ and $\widehat{\Xi}$ are both anti-unitary they can square to $\pm I$ or 0, while $\widehat{\Pi}$ can only square to I or 0. Usually $\pm I$ is simply denoted as ± 1.

The proceeding analysis is concerned with determining the symmetries of Eq. 4.1. If we can find operators satisfying the conditions in Table 1 the corresponding symmetry is present. To do so it is useful to study the 1D case, where Eq. 4.2 reduces to

$$H_\sigma = (\varepsilon_{\mathbf{k}} - \mu)\tau_z + \sigma 2d\sin(k_x)\tau_x\,. \tag{4.3}$$

We immediately find that $\{H_\sigma, \tau_y\} = 0$ and since τ_y is unitary, we can identify $\widehat{\Pi} = \tau_y$. We further observe that $H_\sigma^* = H_\sigma$ and by defining $\widehat{K}$ to denote complex conjugation we find $[H_\sigma, \widehat{K}] = 0$ and can identify $\widehat{\Theta} = \widehat{K}$. Finally we use the relation $\widehat{\Pi} = \widehat{\Xi}\widehat{\Theta}$ [13] to identify $\widehat{\Xi} = \tau_y\widehat{K}$, which is indeed anti-unitary. Furthermore we find $\{H_\sigma, \tau_y\widehat{K}\} = 0$. These three commutator/anti-commutator relations reveal all three symmetries to be present.

This classifies the Hamiltonian in Eq. 4.3 to be BDI, see Table 2. Due to its dimensionality ($d = 1$) we find the that a $\mathbb{Z}$ topological invariant can be defined and the Hamiltonian is said to exhibit non-trivial topological properties. Before proceeding the discussion to these topological invariants we have yet to determine the class of our full Hamiltonian in Eq. 4.2. Checking the commutator and anti-commutators of this Hamiltonian with the predefined operators classifies it to be class D. Since we have one block for each value of σ we say it is class D+D, where each block has an associated $\mathbb{Z}$ topological invariant.

Symmetry				d							
AZ	Θ^2	Ξ^2	Π^2	1	2	3	4	5	6	7	8
A	0	0	0	0	$\mathbb{Z}$	0	$\mathbb{Z}$	0	$\mathbb{Z}$	0	$\mathbb{Z}$
AIII	0	0	1	$\mathbb{Z}$	0	$\mathbb{Z}$	0	$\mathbb{Z}$	0	$\mathbb{Z}$	0
AI	1	0	0	0	0	0	$\mathbb{Z}$	0	$\mathbb{Z}_2$	$\mathbb{Z}_2$	$\mathbb{Z}$
BDI	1	1	1	$\mathbb{Z}$	0	0	0	$\mathbb{Z}$	0	$\mathbb{Z}_2$	$\mathbb{Z}_2$
D	0	1	0	$\mathbb{Z}_2$	$\mathbb{Z}$	0	0	0	$\mathbb{Z}$	0	$\mathbb{Z}_2$
DIII	-1	1	1	$\mathbb{Z}_2$	$\mathbb{Z}_2$	$\mathbb{Z}$	0	0	0	$\mathbb{Z}$	0
AII	-1	0	0	0	$\mathbb{Z}_2$	$\mathbb{Z}_2$	$\mathbb{Z}$	0	0	0	$\mathbb{Z}$
CII	-1	-1	1	$\mathbb{Z}$	0	$\mathbb{Z}_2$	$\mathbb{Z}_2$	$\mathbb{Z}$	0	0	0
C	0	-1	0	0	$\mathbb{Z}$	0	$\mathbb{Z}_2$	$\mathbb{Z}_2$	$\mathbb{Z}$	0	0
CI	1	-1	1	0	0	$\mathbb{Z}$	0	$\mathbb{Z}_2$	$\mathbb{Z}_2$	$\mathbb{Z}$	0

Table 2: The ten classes associated with the three symmetry operators categorized according to the values of the operators squared, where $\pm 1 = \pm I$. Θ and Ξ are anti-unitary and can square to -1 while Π can only square to 0 or 1. d is the dimensionality of the system, and $\mathbb{Z}$ ($\mathbb{Z}_2$) denotes whether a topological invariant can be defined. The table is adopted from [13].

4.1 Topological Invariant

Having classified the Hamiltonian in question we have left to define and compute a topological invariant to count the possible number of Majorana modes. The following quantity,

$$N = \frac{1}{4\pi} \int \mathrm{d}\mathbf{k}\ \hat{\mathbf{g}}(\mathbf{k}) \cdot \left(\frac{\partial \hat{\mathbf{g}}}{\partial k_x} \times \frac{\partial \hat{\mathbf{g}}}{\partial k_y} \right), \tag{4.4}$$

is an integer and constitutes a topological invariant when $\mathbf{g} = (\sigma 2d \sin(k_x), -\sigma 2d \sin(k_y), (\varepsilon_{\mathbf{k}} - \mu))$ so that $H = \mathbf{g} \cdot \boldsymbol{\tau}$ [13]. The integrand in Eq. 4.4 has sharp peaks at the four possible gap closings $((k_x, k_y) = (0,0), (0,\pi), (\pi,0), (\pi,\pi))$, thus it is sufficient to evaluate $\mathbf{g}$ at these four points of the Brillouin zone. To further simplify, we linearize the integrand at each point yielding for instance $\mathbf{g}(0,0) = (\sigma 2dk_x, -\sigma 2dk_y, \varepsilon_{\mathbf{k}} - \mu)$. Additionally, due to the sharp peaks at the gap closings, we can extend the integration limits to all space. Finally we use that the collected factor of $|\mathbf{g}|^{-3}$ can be multiplied onto the integrand after performing the partial derivatives. With these tricks imposed we can solve Eq. 4.4 to find

$$N = \frac{1}{2} sign(4t + \mu) - sign(\mu) - \frac{1}{2} sign(4t - \mu)\,.$$

Thus when $\mu = \pm 4t, 0$ the topological invariant can change. Evaluating the result at $\mu = -\infty, -2t, 2t, \infty$ yields the spectrum seen in Fig. 4. Apparently all values of N lie within $\mathbb{Z}_2$ although they are in principle allowed to take any value belonging to $\mathbb{Z}$. However the low values of N are solely due to the constraints imposed in our model. Had we for instance chosen to include only next-next-nearest neighbor sites in the superconducting coupling such that $d_{\mathbf{k}} = 2d(sin(2k_x) + isin(2k_y))$ this would yield $N = \pm 2$ or 0. This choice of coupling clearly has no physical justification but merely argues that the values of N are indeed $\mathbb{Z}$ and not $\mathbb{Z}_2$ regardless of the opposing implication of Fig. 4. From the result in Fig. 4 we find that as long as $|\mu| < 4t$ our system is in a topologically non-trivial state, and thus allows for one Majorana mode per edge per block.

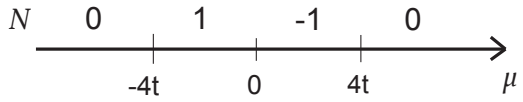

Figure 4: The topological invariant's computed values within the energy regions of the chemical potential. Topological transitions occur at $\mu = \pm 4t$ and $\mu = 0$ as expected. The system exhibits non-trivial topological phases if $|\mu| < 4t$.

4.2 Defects and Topological Classification

In the results analysis in Section 5 the consequences of imposing a regular vortex as well as a half-quantum vortex will be investigated. Such exotic features are not covered by this very general topological classification. Thus a brief overview of the idea behind classification of systems with defects is required before the results are presented. Based on the framework developed in [14] we learn that the overall dimension of the system alone can no longer classify it. Instead we consider a general Hamiltonian $H(\mathbf{k}, \mathbf{r})$ and introduce $\delta = d - D$, where d is still the dimension of the Brillouin zone upon which $\mathbf{k}$ is defined ($d = 2$) while D is the dimension a surface S^D surrounding the defect upon which $\mathbf{r}$ is defined ($D = 1$ for a vortex) [14]. In the 2D $p_x + ip_y$ case (class D+D) we find that with a vortex placed in the system, it is now characterized by a $\mathbb{Z}_2$ topological invariant determining the presence or absence of a Majorana bound state in the vortex core. The new topological invariant can be written $\nu = Nm \mod 2$, where N is the topological invariant computed in the previous subsection, while m is the phase winding number of the vortex. In our case we will impose a vortex winding of $+2\pi$ which corresponds to $m = 1$. Thus we conclude that we should see one bound state at the vortex core for each block, as long as $|\mu| < 4t$.

5 Results

With the necessary theory and derivations in place, we are now ready to investigate solutions to the $p_x + ip_y$ superconductor with triplet OP $\mathbf{d} = (0, 0, d_{ji})$. This section will present results with $t = 1.0$, $\mu = -2.5\,t$, $g = 2\,t$, $\beta = 10\,t^{-1}$, while the size of the system will vary.

5.1 Edge States

The aim is to obtain excitations within the superconducting gap and the simplest way to do so is to apply open boundary conditions (OBC) as described in the discussion of Fig. 2. Thus we consider a strip with periodic boundary conditions (PBC) along the x-direction and OBC along the y-direction. The PBC are imposed by performing a Fourier transform along x yielding a k_x dependence in the energies. The BdG equation is then solved self-consistently for each value of k_x with the usual parameter values. In Fig. 5 the result is shown for $N_y = N = 100$. The top figure shows the excitation energies as a function of k_x, while the bottom figure shows the integrated LDOS within the gap plotted as a function of N.

The first important note is that the energies of the excited quasiparticles hybridize into bands dispersing across the gap, leaving only a single zero-energy mode at exactly $k_x = 0$ per band. This should be of no surprise, since the fermionic nature of the quasiparticles imposes Pauli's exclusion principle. Thus the quasiparticles pair up and divide symmetrically around $E = 0$ leaving the total energy of the states to be 0 as required from the discussion in Section 2.3.

Furthermore the two branches confirm the predicted result obtained in Section 4.1, namely that one

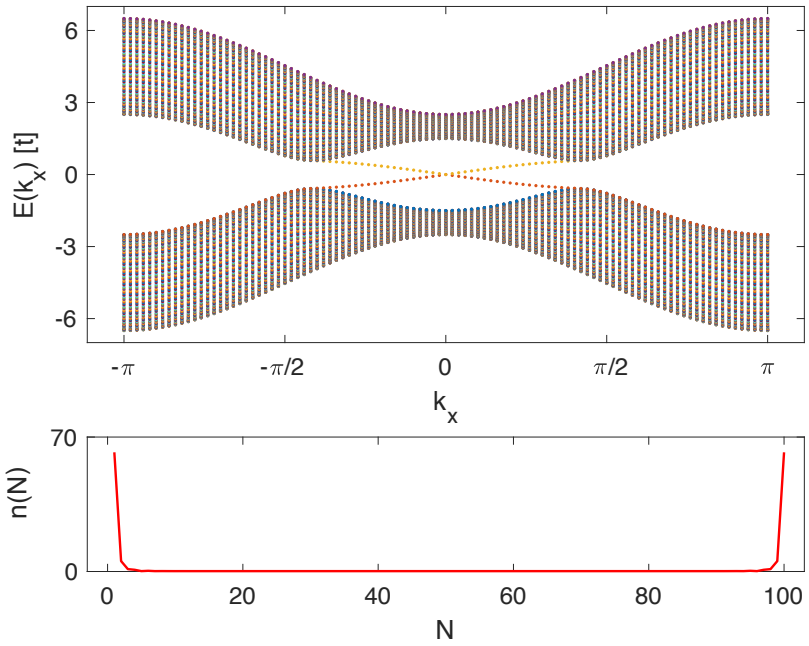

Figure 5: Energy dispersion and the integrated LDOS, $n(N)$, obtained from applying PBC along x and OBC along y. This solution has been computed self-consistently for one block of the Hamiltonian. Top figure verifies the two predicted chiral edge modes, one at each edge, where the quasiparticle states have hybridized into bands. The slopes confirm the presence of edge currents. Bottom figure is the number of in-gap excitations as a function of N. It supports the edge localization of the modes.

mode of quasiparticle states within the gap emerges at each edge. This localization of the modes is confirmed by the integrated LDOS plotted in the bottom figure. In principle the energies of the top figure are two-fold degenerate (recall class D+D) but due to this degeneracy we only solve one block of the Hamiltonian. We further note that the slope of the branches indicates edge currents (since $\mathbf{v} = \partial\varepsilon/\partial\mathbf{k}$) which should indeed be present in a chiral p-wave superconductor as briefly mentioned in Section 2.2. It is possible to have several chiral edge modes if a system of higher chirality is considered (recall chirality $+1$ of our model) such as d- or f-wave superconductors [8, 15]. The results presented in Fig. 5 are in very good agreement with the ones presented in [8].

We further wish to consider results obtained from applying OBC in both directions, see Fig. 6. The results were computed with $N = 51$.

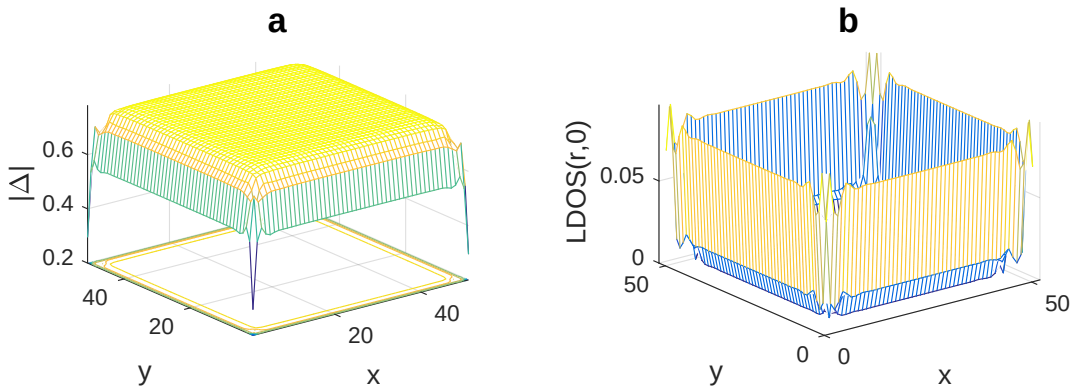

Figure 6: PP amplitude, **a**, and LDOS at zero energy, **b**, with OBC in both directions. The PP is suppressed along the edges indicating the expected localization. The LDOS confirms the presence of edge states and further displays hybridization all along the edge. This suggests no excitation at exactly zero energy, but a non-zero LDOS at all energies within the gap, see Fig. 10 to verify. These results were computed with $N = 51$.

Fig. 6a presents the amplitude of the PP which is suppressed along the boundaries. This behavior indicates the presence of states all along the edges. Fig. 6b, which presents the LDOS at zero energy, confirms this indication. As opposed to Fig. 5 all excitations hybridize into bands yielding no single-site localized state at zero energy but a small, yet distinctly non-zero, LDOS at all edge sites. This behavior of the LDOS repeats itself within the entire superconducting gap. Thus the predicted presence of edge states in the case with OBC along one or two directions is confirmed.

5.2 Vortices

By applying an external magnetic field to a type II superconductor, the magnetic flux can penetrate the superconductor and form an Abrikosov vortex lattice in a vortex state [2]. This occurs when the strength of the magnetic field demands energetically costly supercurrents to eject the field. It thus becomes favorable for the superconductor to suppress the superconducting OP in limited areas (vortices), allowing magnetic flux quanta to penetrate the region. The vortex core is surrounded by supercurrents to restore the superconductivity to the bulk value in the remaining material. In this thesis we will not discuss the critical fields related to the emergence of such a vortex, but solely investigate the consequences thereof.

5.2.1 Caroli-de Gennes-Matricon Vortex Core Levels

When the superconducting OP is suppressed this naturally allows for quasiparticle states within the gap. To briefly discuss the study and particularly the result obtained by Caroli, de Gennes and Matricon, we consider the more common (and manifestly simpler) s-wave superconductor. Allowing the OP to vary as we approach the vortex and rewriting it in polar coordinates yields

$$\Delta(\mathbf{r}) = \Delta(r)e^{i\theta}. \tag{5.1}$$

With this one can redefine the eigenfunctions and thus the BdG equation itself. By assuming the shape of the OP as depicted in Fig. 7, the new BdG equation can be solved analytically. It is done by introducing a radius r_C very close to the vortex core and considering the two regions $r < r_C$ (where $\Delta(r)$ is neglected completely) and $r > r_C$ followed by matching the two solutions at the boundary $r = r_C$.
Caroli, Matricon and de Gennes found

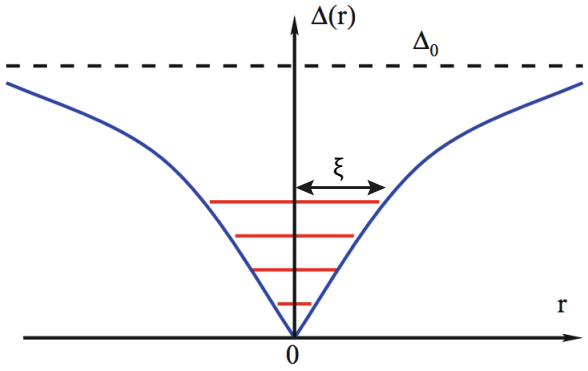

Figure 7: Illustration of the behavior of the OP around a single, isolated vortex, where Δ_0 is the bulk value. The OP is suppressed as the vortex is approached and ultimately zero in the vortex core. ξ is the coherence length defining the width of the vortex and the red lines illustrate the CdGM bound states in the vortex core. The figure is adopted from [16]

$$E_m = m\frac{\Delta_0^2}{\varepsilon_F} \tag{5.2}$$

in the limit where $\varepsilon_F >> \Delta_0$. m is a half-integer [6] and Δ_0 is, as seen in Fig. 7, the bulk value of the OP [16]. This result yields several energy levels within the vortex, one for each m. These are known as Caroli-de Gennes-Matricon levels (CdGM) and illustrated by red lines in the figure. The distance between the levels is $\varepsilon_C = \Delta_0^2/\varepsilon_F$ and the lowest lying level has $m = 1/2$. The full derivation can be seen in [16, 18]. Naturally this distance must be affected by the width of the vortex, which is defined by the coherence length, $\xi = \hbar v_F/2\Delta_0$. As one might expect, a large zero-energy coherence length corresponds to close lying core levels, and the discretization is in practice thermally smeared, while a short zero-energy coherence length yields a noticeable distinction [16].
To verify the prediction of the CdGM bound states, a simulation of an s-wave superconductor with a vortex enforced in the center has been performed. The result can be seen in Fig. 8. The computation was performed without self-consistency and with $N = 40$. The vortex is imposed by setting $\Delta(r) = 0$ at the four central sites, which corresponds to setting r_C to be the radius of a circle surrounding these. A phase, $e^{i\theta(\mathbf{r})}$, was applied to the remaining sites by inserting a coordinate system with origin in the vortex core, where $\theta(\mathbf{r})$ is the angle from the x-axis to the position of the given site, naturally ranging from 0 to 2π. This corresponds to a winding of $+2\pi$ which can also be denoted as vorticity $+1$. It is possible to consider cases with higher vorticity corresponding to stronger supercurrents, hence several flux quanta passing through the vortex.

Fig. 8a presents the core LDOS within the gap with $\Delta_0 = 0.4$. In this case there are several in-gap states at distinctly separated energies as predicted. Fig. 8b, having $\Delta_0 = 0.1$, does not yield this discretization. This is due to the low OP, since it corresponds to a large coherence length resulting in a smearing of the LDOS. However with $\Delta_0 = 0.1$ we are on the boarder of satisfying $\varepsilon_F >> \Delta_0$

[6] m is actually the azimuthal angular momentum of monopole harmonics, but since we have not gone into detail with the derivation, this statement may confuse the reader. For our purposes it is sufficient to be aware of the half-integer restriction. The interested reader is referred to [16–18].

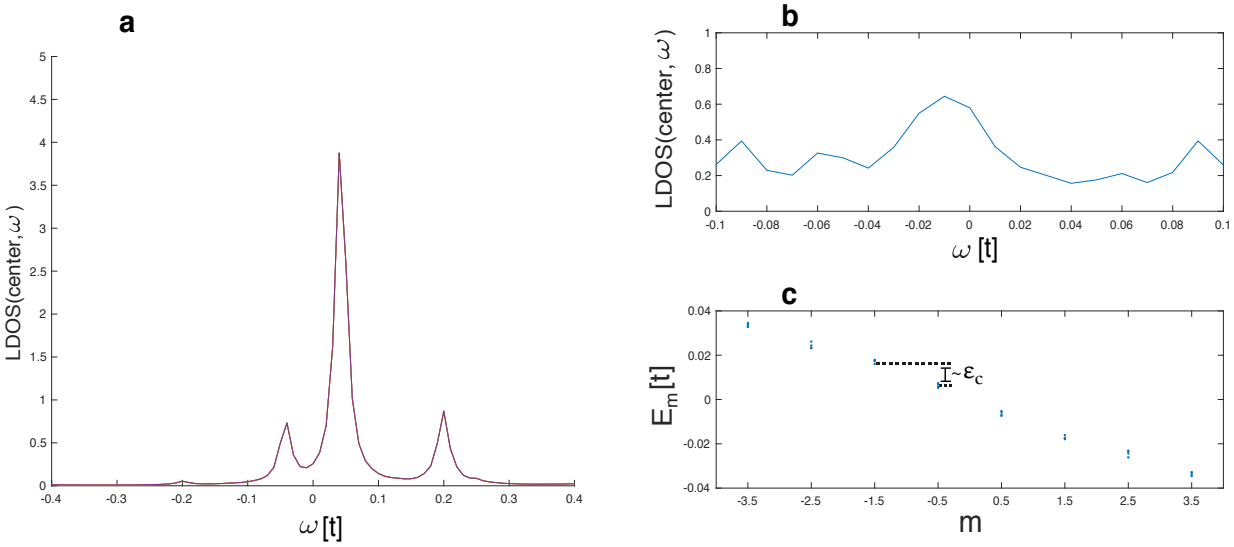

Figure 8: Results for a simple, isolated vortex in the center of an s-wave superconductor. **a** shows the LDOS of the vortex core with $\Delta_0 = 0.4$. There are several excitations at distinct energies within the gap. **b** shows the LDOS of the vortex core with $\Delta_0 = 0.1$. The discretization of the excitations has been smeared out due to the large coherence length. Only the energies within the superconducting gap are included in **a** and **b**. **c** is the excitation energies as a function of m. The levels yield a separation of the order of ε_C as predicted from Eq. 5.2. In **a** and **c** it is evident that there are no zero-energy excitations. All three figures have been computed non-self-consistently with $N = 40$.

($\varepsilon_F = 1.5$), thus the mid-gap states should yield levels resembling Eq. 5.2. A thorough analysis of this assertion has been performed in [17], where a spherical symmetric system with a vortex-antivortex pair is considered. This symmetry allows m to be a good quantum number, enabling a diagonalization of the BdG equation separately for each m. This is obviously in contrast to our grid model, thus we merely compare the qualitative resemblance of the two results.
In Fig. 8c we have plotted the mid-gap excitation energy levels, where we imposed the assumed dependence of m predicted by theory. First and foremost we can confirm the overall level splitting, since the excitations collect in separate groups of four at distinct energies. Furthermore the order of the discretization is indeed the same as the order of ε_C and the levels divide symmetrically around $E_m = 0$ with no exact zero-energy state. There is a great resemblance to Fig. 6 in [17] with a discrepancy regarding the degeneracy [7] due to the vast differences in the models considered. We can conclude that by imposing a simple, isolated vortex in an s-wave superconductor, several in-gap states emerge symmetrically around $E = 0$, while no exact zero-energy state will be present.

5.2.2 Vortex in a $p_x + ip_y$ Superconductor

With the theory concerning bound states in vortex cores of s-wave superconductors in mind, we can now investigate the more complicated case of the $p_x + ip_y$ superconductor with a simple, isolated vortex, which cannot be solved analytically. The vortex has once again been enforced by applying a phase to all sites. Each intersite superconducting coupling has then been assigned to a corresponding site, such that the coupling between j and $j+\hat{x}$ as well as j and $j+\hat{y}$ corresponds to the phase at site j, while the remaining two interactions obtain a phase defined by site $j-\hat{x}$ and $j-\hat{y}$ respectively. There is no need to force the OP to 0 at any sites, since the PP is suppressed due to intersite interaction. The PP and LDOS($\mathbf{r}$,0) are presented in Fig. 9. The results have been computed with OBC, and the triplet OP has been found self-consistently as usual. In 9a the PP is shown. Comparing this to the

[7] Four-fold in our case, doubly in [17].

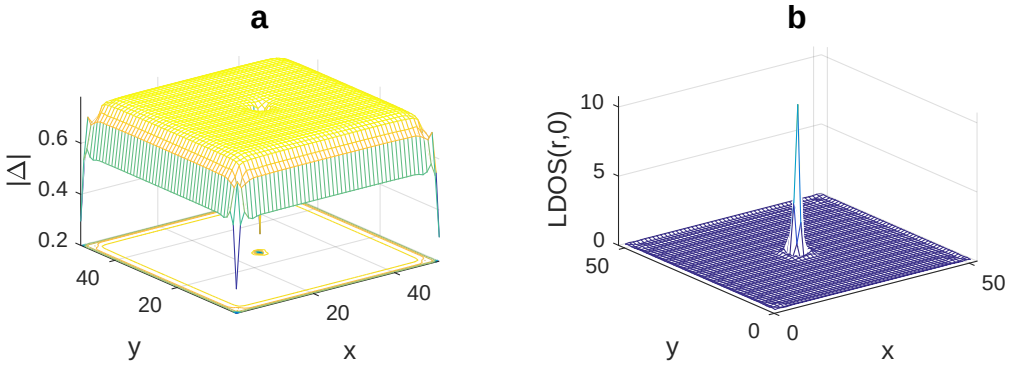

Figure 9: PP amplitude (**a**) and LDOS (**b**) at zero energy for a p_x+ip_y superconductor with OBC and a vortex at the center site. The PP is strongly suppressed at the vortex and moderately suppressed along the boundaries. The LDOS shows a highly localized zero-energy excitation in the vortex core and vanishing amplitude along the boundaries.

PP seen in Fig. 6a we note that there is an additional strong decrease surrounding the vortex core, while the edges are equally suppressed with and without a vortex. The computation has $N = 51$, thus the vortex is narrowly centered at one site. Due to the non-trivial topology of the $p_x + ip_y$ superconductor a zero-energy quasiparticle is attainable. Fig. 9b shows the LDOS at zero-energy, and we note that a highly localized zero-energy excitation has indeed emerged in the vortex core. The edge states discussed in Section 5.1 are still present, but due to their hybridized energies the LDOS at the edges is vanishing compared to the vortex core state.

To further compare the case of a $p_x + ip_y$ superconductor with a vortex to previous results, we consider Fig. 10. Figs. **a, b** and **c** present the LDOS in the case with OBC and a vortex, **d, e** and **f** are the results from the case with OBC but without a vortex and finally **g, h** and **i** are computed with PBC also without a vortex. Top row is the LDOS of the site in the vortex core, where **d, g** verify a full gap in the absence of a vortex, while **a** confirms the highly localized zero-energy state. Interestingly we note that this is the only excitation in the core. This result is in great agreement with the results presented in [2, 12]. Middle row is the LDOS of a site situated between the vortex and the edge. All three plots present clear evidence of a full gap. Bottom row is the LDOS of a site situated at the middle of one edge. Figs. **c** and **f** are practically identical but with a slightly larger LDOS of near-zero-energy states in the case without a vortex. This is most likely due to the fact that the zero-energy excitation in the core does not hybridize with the edge states. Finally Fig. 10i once again confirms a full gap in the case of PBC. The result in Fig. 10a is in strong contrast to the s-wave case discussed in the previous section, where no zero-energy excitation is present, but several in-gap states appear. Distinct CdGM levels can still emerge in the p-wave case by widening the vortex. This can be done by setting the OP to 0 at several central sites as done in the s-wave case. However the guaranteed emergence of a zero-energy bound state in the vortex core is intrinsic only to the p-wave superconductor and is one of its known exotic features [2, 8, 17].

This concludes the discussion of vortices with the regular winding of $+2\pi$ (vorticity $+1$). Up until now the term MF has been carefully avoided. A key property of a such is that $\gamma_{i\sigma} = \gamma_{i\sigma}^\dagger$ and we have thus far considered the spinful case of a $p_x + ip_y$ superconductor, where the triplet OP has $d_x = d_y = 0$. This implies a Bogoliubov transformation as described in Eq. 3.6, where regardless of $u_{p\varepsilon\sigma} = v_{p\varepsilon\sigma}$, $\gamma_{i\sigma} \neq \gamma_{i\sigma}^\dagger$ due to the spin dependence of the operators. Thus the zero-energy excitations are not Majorana zero modes [8]. However in this spinful case the possibility of a half-quantum vortex (HQV) has been predicted to host a true, robust Majorana zero-mode [6, 8].

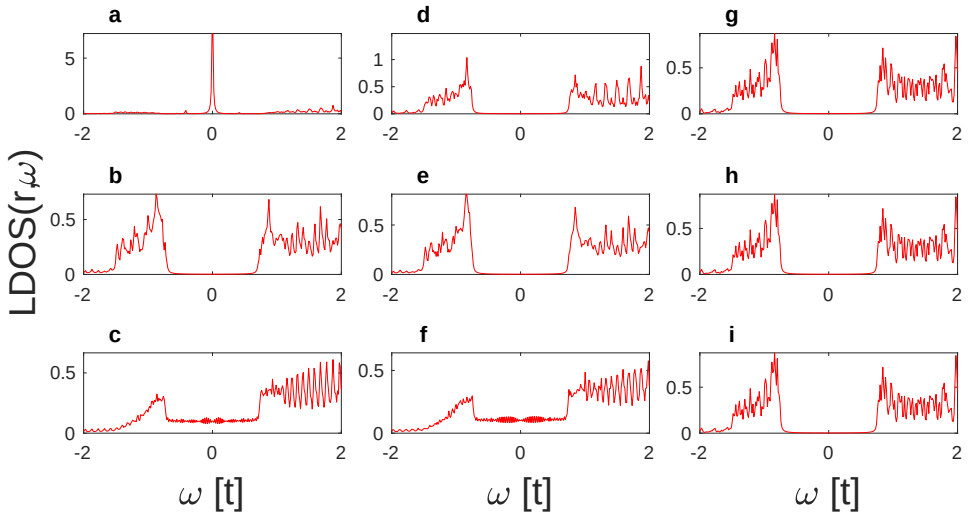

Figure 10: The LDOS in the case of OBC with a vortex (**a b c**), OBC without a vortex (**d e f**) and PBC also without a vortex (**g h i**). Top row is LDOS of the center site, middle row is LDOS of a site between the center and the edge, while bottom row is LDOS of an edge site. These plots were computed with $N = 51$. The center site reveals a full gap with PBC and OBC without vortex, while we see the sharp peak at zero energy when a vortex has been imposed corresponding to a quasiparticle excitation with $E = 0$ in the vortex core. In all three cases there is a full gap at the site between the edge and the core. The edge site has hybridized quasiparticle states in the cases with OBC and a full gap in the case of PBC.

5.3 Half-Quantum Vortex

A HQV can be described as a vortex in only one spin component. Thus we abandon the model discussed so far and now set $d_z = 0$ and $d_x, d_y \neq 0$ to uncouple the spin directions. We will not engage in a detailed discussion on the symmetry groups, but rather give an intuitive understanding of this peculiar phenomenon. The HQV can arise by having a winding $\theta/2 = +\pi$ of the superconducting OP, $\Delta(r)$ (similar to Eq. 5.1 but with half the winding), while a rotation of the **d**-vector is performed simultaneously in the xy-plane. This is done by letting $\hat{d} = \cos(\phi)\hat{x} + \sin(\phi)\hat{y}$, where ϕ changes by π and denotes the angle from the x-axis [19]. Using the original definition of $\hat{\Delta}$ (Eq. 2.8) we immediately find that the Δ^{++} (Δ^{--}) pairing corresponds to $-d_x + id_y = -e^{-i\phi}$ ($d_x + id_y = e^{i\phi}$) coupling, where we imposed the new definition of $\hat{d}$. Hence we can write the full OP as [8]

$$\Delta(r, \phi, \theta) = \Delta(r)e^{i\frac{\theta}{2}}(-e^{-i\phi}\,|\uparrow\uparrow\rangle + e^{i\phi}\,|\downarrow\downarrow\rangle), \tag{5.3}$$

where $\Delta(r)$ is the magnitude of the OP as previously. With this notation it is obvious that the effect of the rotation is to eliminate the phase angle completely from the spin up component, while the spin down component sees an effective winding of $+2\pi$, yielding the usual full single-quantum vortex. Since the magnetic flux penetrating the superconductor only depends on the winding of θ the total flux through the superconductor is $\frac{1}{2}\Phi_0 = h/4e$, hence the name half-quantum vortex [8].
To create a scenario giving rise to a rotation of the **d**-vector can seem far-fetched at first glance, since in general the spin direction will favor an alignment with the orbital momentum due to spin-orbit coupling. Thus the energy cost associated with the rotation is far too large to ever be favorable. However studies suggest that in the $p_x + ip_y$ superconductor Sr_2RuO_4, applying a magnetic field along what is currently believed to be the direction of $\hat{l}$ ($\hat{z}$) which is strong enough to overcome the spin-orbit energy will effectively neutralize the spin-orbit coupling and possibly permit the HQV state to stabilize [6,19].

To solve the described scenario we must naturally redefine the BdG equation, due to the decoupling

of the spin directions. Performing calculations similar to the ones described in Section 3 yields

$$E_{\varepsilon\sigma}\begin{pmatrix} u_{j\varepsilon\sigma} \\ v_{j\varepsilon\sigma} \end{pmatrix} = \sum_i \begin{pmatrix} K_{ji} & -\sigma d_{x,ji} + i d_{y,ji} \\ \sigma d^*_{x,ji} + i d^*_{y,ji} & -K^*_{ji} \end{pmatrix} \begin{pmatrix} u_{i\varepsilon\sigma} \\ v_{i\varepsilon\sigma} \end{pmatrix}, \tag{5.4}$$

where $\sigma = +1(-1)$ for pseudospin up (down). We can solve this separately for each spin component.

In addition to redefining the BdG equation, we should reconsider the classification of the system. Repeating the procedure described in Section 4, we write the new Hamiltonian in terms of the four-Nambu spinor and block diagonalize it, yielding

$$H_\sigma = \sigma(\varepsilon_{\mathbf{k}} - \mu)\tau_z + 2(d_x \sin(k_x) + \sigma d_y \sin(k_y))\tau_x + 2(d_y \sin(k_x) - \sigma d_x \sin(k_y))\tau_y \,,$$

with $\sigma = +1(-1)$ for spin up (down) as previously. Thus the Hamiltonian remains in class D+D with the same operators as identified in Section 4.

To impose the HQV in the solution to the new BdG equation (5.4), we implement the general phase with angle $\theta/2$ in the $\hat{\Delta}$-matrices, while the rotation phases are implemented directly into the BdG-matrices. The result can be seen in Fig. 11, where **a, b** are the solutions to the spin up case and **c, d** are the solutions to the spin down case.

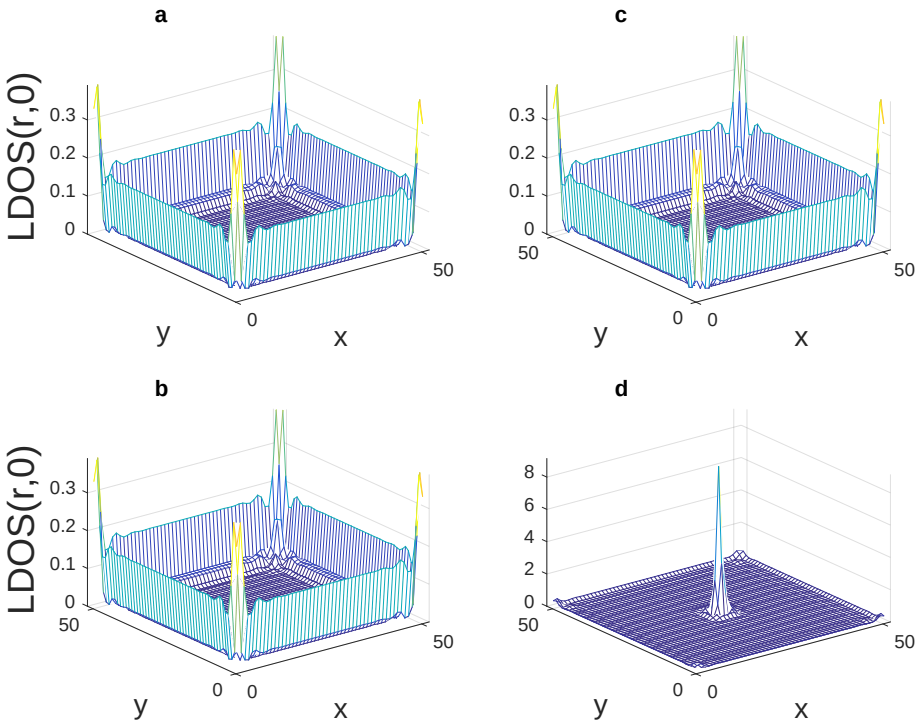

Figure 11: The LDOS of all sites at zero energy. **a** and **b** are solutions to the BdG equation with spin up, while **c** and **d** are solutions to spin down. **a, c** are the cases without a HQV and with OBC. They confirm the expected behavior, where only edge states are present. **c, d** are with OBC and HQV. There is no change in the LDOS of spin up, while the spin down solution has a clear zero-energy excitation. The computation was performed non-self-consistently with $N = 51$, $d_x = 0$ and $d_y = -i0.3$.

All four plots were computed with OBC. **a, c** are the solutions without the HQV and are included solely to verify the expected behavior in this case. Figs. **b, d** clearly show no effects of the vortex

in the spin up case and the usual presence of a zero-energy excitation in the spin down case. The computation was performed non-self-consistently with $N = 51$, $d_x = 0$ and $d_y = -i0.3$. The values of the **d**-components were chosen by considering their original definition in Eq. 3.3b, where one finds $d_{x,ji} = g_{x,ji}(\langle c_{i\downarrow}c_{j\downarrow}\rangle - \langle c_{i\uparrow}c_{j\uparrow}\rangle)$ and $d_{y,ji} = -ig_{y,ji}(\langle c_{i\downarrow}c_{j\downarrow}\rangle + \langle c_{i\uparrow}c_{j\uparrow}\rangle)$. The sign on $d_{y,ji}$ has been adopted from the definition of Δ_{ji} in Eq. 3.3a to match sign of d_y in the general $\hat{\Delta}$-matrix in Eq. 2.8, obviously without any loss of generality. We chose to compute the results for $\langle c_{i\downarrow}c_{j\downarrow}\rangle = \langle c_{i\uparrow}c_{j\uparrow}\rangle$. Not satisfying this equality does not have any effect besides leaving the edge amplitude of LDOS(**r**,0) unequal in the different spin cases.

At first glance, the results in Fig. 11 and Figs. 6 and 9 appear quite similar. However the results have a crucial difference. While redefining our BdG equation, the Bogoliubov transformation used combines creation and annihilation operators of the same species, that is for instance $\gamma_{\varepsilon\downarrow} = \sum_i (u_{i\varepsilon\downarrow}c_{i\downarrow} + v_{i\varepsilon\downarrow}c^\dagger_{i\downarrow})$. Due to particle-hole symmetry this leads to $\gamma_{\varepsilon\downarrow}(-E_\varepsilon) = \gamma^\dagger_{\varepsilon\downarrow}(E_\varepsilon)$, hence at zero energy $\gamma_{\varepsilon\downarrow}(0) = \gamma^\dagger_{\varepsilon\downarrow}(0)$ [19]. Altogether the spin down block of the Hamiltonian considered in the subsection is class D with a point defect. Such a defect is characterized by a $\mathbb{Z}_2$ topological invariant [14]. Since $N = +1$ ($\mu = -2.5t$) and the vorticity of the spin down block is $+1$, $\nu = 1$. Thus we are in a non-trivial topological state allowing a single topologically protected zero-energy excitation in the vortex core. Furthermore we know that this zero-energy excitation is its own antiparticle. Thus we conclude the results presented in this thesis with the half-quantum vortex yielding a possibility of realizing a Majorana bound state in a spinful $p_x + ip_y$ superconductor.

6 Conclusion and Outlook

Throughout this thesis an investigation of a chiral p-wave superconductor has been performed. Due to the non-trivial topology, chiral edge modes emerged within the superconducting gap when finite systems were considered. Furthermore we presented results describing the guaranteed presence of a bound zero-energy excitation in a vortex core of the $p_x + ip_y$ superconductor, which is one of its well-known exotic features. Finally we investigated the consequences of having a half-quantum vortex present at the center site. This investigation led to an interesting phenomenon where a vortex was only seen by one of the spin pairings present in the system. The half-quantum vortex yielded a Majorana bound state in the vortex core.

The stabilization of the half-quantum vortex was briefly discussed during the results presentation. In further works it would be of great interest to conduct an examination of the prospects mentioned. This inquiry could appropriately take its offset in a proper establishment of a regular vortex via the application of a magnetic field rather than the presented enforcement of a phase winding.
A thorough, realistic investigation would further imply the need of considering the material most likely to exhibit the nature discussed throughout this thesis, that is strontium ruthenate. This would demand a consideration of interband interaction and obviously the spin-orbit coupling expected to be problematic with regards to the required rotation of **d** in the formation of the half-quantum vortex.

Altogether this thesis has provided a theoretical explanation of an intrinsic topological superconductor with triplet pairing. The emphasis has been on the exploration of some known exotic features as well as the possible emergence of Majorana zero modes.

References

[1] L P Gor'kov. Exotic superconductors. *Physica Scripta*, 32(1):6, 1985.

[2] Yao-Wu Guo, Wei Li, and Yan Chen. Impurity- and magnetic-field-induced quasiparticle states in chiral p-wave superconductors. *Frontiers of Physics*, 12(5):127403, 2017.

[3] J.F. Annett. *Superconductivity, Superfluids and Condensates*. Oxford Master Series in Physics. OUP Oxford, 2004.

[4] M. T. Mercaldo, M. Cuoco, and P. Kotetes. Magnetic-field-induced topological reorganization of a p -wave superconductor. *Physical Review B*, 94(14):140503, October 2016.

[5] M. Leijnse and K. Flensberg. Introduction to topological superconductivity and Majorana fermions. *Semiconductor Science Technology*, 27(12):124003, December 2012.

[6] S. B. Chung, H. Bluhm, and E.-A. Kim. Stability of Half-Quantum Vortices in p_x+ip_y Superconductors. *Physical Review Letters*, 99(19):197002, November 2007.

[7] Henrik Bruus and Karsten Flensberg. *Many-body quantum theory in condensed matter physics - an introduction*. Oxford University Press, 2004.

[8] Catherine Kallin and John Berlinsky. Chiral superconductors. *Reports on Progress in Physics*, 79(5):054502, 2016.

[9] A.P Mackenzie and Y Maeno. p-wave superconductivity. *Physica B: Condensed Matter*, 280(1–4):148 – 153, 2000.

[10] K. Hashimoto. *Non-Universal Superconducting Gap Structure in Iron-Pnictides Revealed by Magnetic Penetration Depth Measurements*. Springer Theses Series. Springer Customer Service Center Gmbh, 2016.

[11] A. Y. Kitaev. 6. QUANTUM COMPUTING: Unpaired Majorana fermions in quantum wires. *Physics Uspekhi*, 44:131, October 2001.

[12] Mitsuaki Takigawa, Masanori Ichioka, Kazushige Machida, and Manfred Sigrist. Vortex structure in chiral p-wave superconductors. *Phys. Rev. B*, 65:014508, Nov 2001.

[13] Panagiotis Kotetes. Topological insulators and superconductors - notes of tkmi 2013/2014 guest lectures. 2014.

[14] J. C. Y. Teo and C. L. Kane. Topological defects and gapless modes in insulators and superconductors. *Physical Review B*, 82(11):115120, September 2010.

[15] W. Huang, E. Taylor, and C. Kallin. Vanishing edge currents in non-p -wave topological chiral superconductors. *Physical Review B*, 90(22):224519, December 2014.

[16] Jian-Xin Zhu. *Bogoliubov-de Gennes Method and Its Applications*. Lecture Notes in Physics. Springer International Publishing, 2016.

[17] Y. E. Kraus, A. Auerbach, H. A. Fertig, and S. H. Simon. Majorana fermions of a two-dimensional p_x+ip_y superconductor. *Physical Review B*, 79(13):134515, April 2009.

[18] P. G. de Gennes. *Superconductivity of Metals and Alloys*. Advanced Book Classics. Perseus Books, 1966 (1999).

[19] Sankar Das Sarma, Chetan Nayak, and Sumanta Tewari. Proposal to stabilize and detect half-quantum vortices in strontium ruthenate thin films: Non-abelian braiding statistics of vortices in a $p_x + ip_y$ superconductor. *Phys. Rev. B*, 73:220502, Jun 2006.

Appendices

A Derivation of the Bogoliubov-de Gennes Equation

Starting with the Hamiltonian in the form of Eq. 3.5, $H = H^0 + H^\Delta$, the goal is to use the spin-generalized Bogoliubov transformation to obtain the BdG equation. This is most commonly done by calculating the commutator of H and $c_{p\sigma}$ in different bases and equating the two, where p and σ is site and spin indices respectively. Thus we begin by calculating

$$\begin{aligned}
[H^0, c_{p\sigma}] &= -\sum_{i,j,\alpha}(t_{i,j} + \mu\delta_{ij})[c^\dagger_{i\alpha}c_{j\alpha}, c_{p\sigma}] \\
&= -\sum_{i,j,\alpha}(t_{i,j} + \mu\delta_{ij})(c^\dagger_{i\alpha}\{c_{j\alpha}, c_{p\sigma}\} - \{c^\dagger_{i\alpha}, c_{p\sigma}\}c_{j\alpha})
\end{aligned}$$

Using the fermion anticommutator relations, $\{c_\nu, c_\mu\} = \{c^\dagger_\nu, c^\dagger_\mu\} = 0$ and $\{c^\dagger_\nu, c_\mu\} = \delta_{\mu\nu}$, we obtain

$$\begin{aligned}
[H^0, c_{p\sigma}] &= \sum_{i,j,\alpha}(t_{i,j} + \mu\delta_{ij})\delta_{ip}\delta_{\alpha\sigma}c_{j\alpha} \\
&= \sum_j (t_{p,j} + \mu\delta_{pj})c_{j\sigma}
\end{aligned} \tag{A.1}$$

And

$$\begin{aligned}
[H^\Delta, c_{p\sigma}] &= \sum_{i,j}\left(d_{ji}[c^\dagger_{j\sigma}c^\dagger_{i-\sigma}, c_{p\sigma}] + d^\dagger_{ji}[c_{i-\sigma}c_{j\sigma}, c_{p\sigma}]\right) \\
&= \sum_{i,j} d_{ji}\left(c^\dagger_{j\sigma}\{c^\dagger_{i-\sigma}, c_{p\sigma}\} - \{c^\dagger_{j\sigma}, c_{p\sigma}\}c^\dagger_{i-\sigma}\right) \\
&= -\sum_{i,j} d_{ji}\delta_{jp}c^\dagger_{i-\sigma} \\
&= -\sum_i d_{pi}c^\dagger_{i-\sigma} \\
&= \sum_j d_{jp}c^\dagger_{j-\sigma}
\end{aligned} \tag{A.2}$$

Combining Eqs. A.1 and A.2 we find,

$$[H, c_{p\sigma}] = \sum_j \left[(t_{p,j} + \mu\delta_{pj})c_{j\sigma} + d_{jp}c^\dagger_{j-\sigma}\right] \tag{A.3}$$

Now introducing the previously mentioned spin-generalized Bogoliubov transformation,

$$\begin{pmatrix} c_{p\sigma} \\ c^\dagger_{p-\sigma} \end{pmatrix} = \sum_{\varepsilon>0}\begin{pmatrix} u_{p\epsilon\sigma} & v^*_{p\epsilon\sigma} \\ v_{p\epsilon-\sigma} & u^*_{p\epsilon-\sigma} \end{pmatrix}\begin{pmatrix} \gamma_{\epsilon\sigma} \\ \gamma^\dagger_{\epsilon-\sigma} \end{pmatrix} \tag{A.4}$$

where the summation over ε must be chosen to cover half of the eigenstates since the transformation itself should not introduce twice the number of states in the system. From now on this restriction on the sum will not be written explicitly. The transformation allow us to rewrite Eq. A.3 to

$$\begin{aligned}
[H, c_{p\sigma}] &= \sum_j \left[(t_{p,j} + \mu\delta_{pj})\sum_\varepsilon\left(u_{j\varepsilon\sigma}\gamma_{\varepsilon\sigma} + v^*_{j\varepsilon\sigma}\gamma^\dagger_{\varepsilon-\sigma}\right) + d_{jp}\sum_\varepsilon\left(u^*_{j\varepsilon-\sigma}\gamma^\dagger_{\varepsilon-\sigma} + v_{j\varepsilon-\sigma}\gamma_{\varepsilon\sigma}\right)\right] \\
&= \sum_{\varepsilon,j}\left[\left((t_{p,j} + \mu\delta_{pj})u_{j\varepsilon\sigma} + d_{jp}v_{j\varepsilon-\sigma}\right)\gamma_{\varepsilon\sigma} + \left((t_{p,j} + \mu\delta_{pj})v^*_{j\varepsilon\sigma} + d_{jp}u^*_{j\varepsilon-\sigma}\right)\gamma^\dagger_{\varepsilon-\sigma}\right]
\end{aligned} \tag{A.5}$$

The point of introducing the new basis, is to demand H to be diagonal in this basis, since the transformation matrix is unitary, this can be expressed as $UHU^\dagger = \tilde{H}$, where $U = \begin{pmatrix} u_{p\epsilon\sigma} & v^*_{p\epsilon\sigma} \\ v_{p\epsilon-\sigma} & u^*_{p\epsilon-\sigma} \end{pmatrix}$.

Thus $\tilde{H}$ is expressed in the γ-basis as follows,

$$\tilde{H} = E_0 + \sum_{\varepsilon\sigma} E_{\varepsilon\sigma}\gamma^\dagger_{\varepsilon\sigma}\gamma_{\varepsilon\sigma} \tag{A.6}$$

Where E_0 is the ground state energy of the system. Notice that the γ operators creates (annihilates) excitations of non-interacting fermionic quasiparticles *above* the ground state.

The next step is to obtain $[\tilde{H}, c_{p\sigma}]$, where we drop the E_0 term since this is a scalar and will trivially commute with any operator.

$$\begin{aligned}
[\tilde{H}, c_{p\sigma}] &= \Big[\tilde{H}, \sum_{\varepsilon}\Big(u_{p\varepsilon\sigma}\gamma_{\varepsilon\sigma} + v^*_{p\varepsilon\sigma}\gamma^\dagger_{\varepsilon-\sigma}\Big)\Big] \\
&= \sum_{\varepsilon}\Big(u_{p\varepsilon\sigma}[\tilde{H}, \gamma_{\varepsilon\sigma}] + v^*_{p\varepsilon\sigma}[\tilde{H}, \gamma^\dagger_{\varepsilon-\sigma}]\Big) \\
&= \sum_{\varepsilon}\Big(-u_{p\varepsilon\sigma}E_{\varepsilon\sigma}\gamma_{\varepsilon\sigma} + v^*_{p\varepsilon\sigma}E_{\varepsilon-\sigma}\gamma^\dagger_{\varepsilon-\sigma}\Big)
\end{aligned} \tag{A.7}$$

Where we used that

$$\begin{aligned}
[\tilde{H}, \gamma_{\varepsilon\sigma}] &= \sum_{\tilde{\varepsilon},\alpha} E_{\tilde{\varepsilon}\alpha}[\gamma^\dagger_{\tilde{\varepsilon}\alpha}\gamma_{\tilde{\varepsilon}\alpha}, \gamma_{\varepsilon\sigma}] \\
&= \sum_{\tilde{\varepsilon},\alpha} E_{\tilde{\varepsilon}\alpha}\Big(\gamma^\dagger_{\tilde{\varepsilon}\alpha}\{\gamma_{\tilde{\varepsilon}\alpha}, \gamma_{\varepsilon\sigma}\} - \{\gamma^\dagger_{\tilde{\varepsilon}\alpha}, \gamma_{\varepsilon\sigma}\}\gamma_{\tilde{\varepsilon}\alpha}\Big) \\
&= -\sum_{\tilde{\varepsilon},\alpha} E_{\tilde{\varepsilon}\alpha}\delta_{\varepsilon\tilde{\varepsilon}}\delta_{\alpha\sigma} \\
&= -E_{\varepsilon\sigma}\gamma_{\varepsilon\sigma}
\end{aligned}$$

Similarly we find,

$$[\tilde{H}, \gamma^\dagger_{\varepsilon\sigma}] = E_{\varepsilon\sigma}\gamma^\dagger_{\varepsilon\sigma}$$

Equating Eqs. A.5 and A.7 and separating into equations in $\gamma_{\varepsilon\sigma}$ and $\gamma^\dagger_{\varepsilon-\sigma}$ respectively yields

$$-E_{\varepsilon\sigma}u_{p\varepsilon\sigma} = \sum_j \left((t_{p,j} + \mu\delta_{pj})u_{j\varepsilon\sigma} + d_{jp}v_{j\varepsilon-\sigma}\right) \tag{A.8}$$

$$E_{\varepsilon-\sigma}v^*_{p\varepsilon\sigma} = \sum_j \left((t_{p,j} + \mu\delta_{pj})v^*_{j\varepsilon\sigma} + d_{jp}u^*_{j\varepsilon-\sigma}\right) \tag{A.9}$$

Exchanging $j \to i$ and $p \to j$ in Eq. A.8 gives

$$\begin{aligned}
E_{\varepsilon\sigma}u_{j\varepsilon\sigma} &= \sum_i \left((-t_{j,i} - \mu\delta_{ji})u_{i\varepsilon\sigma} - d_{ij}v_{i\varepsilon-\sigma}\right) \\
E_{\varepsilon\sigma}u_{j\varepsilon\sigma} &= \sum_i \left((-t_{j,i} - \mu\delta_{ji})u_{i\varepsilon\sigma} + d_{ji}v_{i\varepsilon-\sigma}\right)
\end{aligned} \tag{A.10}$$

Where we exploited the antisymmetry of d_{ji} in the second line. Complex conjugating Eq. A.8 gives

$$E^*_{\varepsilon-\sigma}v_{p\varepsilon\sigma} = \sum_j \left((t^*_{p,j} + \mu^*\delta_{pj})v_{j\varepsilon\sigma} + d^*_{jp}u_{j\varepsilon-\sigma}\right)$$

Using that $E^*_{\varepsilon-\sigma} = E_{\varepsilon-\sigma}$, since this is an eigenenergy of the system, hence it must be real, and identifying $d^*_{jp} = d^\dagger_{jp}$ in Eq. A.9 gives

$$E_{\varepsilon-\sigma} v_{p\varepsilon\sigma} = \sum_j \left((t^*_{p,j} + \mu^* \delta_{pj}) v_{j\varepsilon\sigma} + d^\dagger_{jp} u_{j\varepsilon-\sigma} \right)$$

Again exchanging $p \to j$ and $j \to i$ as well as $\sigma \to -\sigma$, we get

$$E_{\varepsilon\sigma} v_{j\varepsilon-\sigma} = \sum_i \left((t^*_{j,i} + \mu^* \delta_{ji}) v_{i\varepsilon-\sigma} + d^\dagger_{ij} u_{i\varepsilon\sigma} \right) \tag{A.11}$$

$$= \sum_i \left((t^*_{j,i} + \mu^* \delta_{ji}) v_{i\varepsilon-\sigma} - d^\dagger_{ji} u_{i\varepsilon\sigma} \right) \tag{A.12}$$

Finally taking Eqs. A.10 and A.12 and rewriting them into matrix form, we obtain the Bogoliubov-de Gennes equation

$$E_\varepsilon \begin{pmatrix} u_{j\varepsilon\sigma} \\ v_{j\varepsilon-\sigma} \end{pmatrix} = \sum_i \begin{pmatrix} K_{ji} & d_{ji} \\ -d^\dagger_{ji} & -K^*_{ji} \end{pmatrix} \begin{pmatrix} u_{i\varepsilon\sigma} \\ v_{i\varepsilon-\sigma} \end{pmatrix}, \tag{A.13}$$

where $K_{ji} = -t_{j,i} - \mu\delta_{ji}$. The spin index on the energies has been dropped, since they are spin degenerate. Eq. A.13 yields a self-consistent eigenvalue problem, which has been solved numerically.

B Fourier Transform

We consider the Hamiltonian

$$H = \underbrace{-t\sum_{i,j,\alpha} c^\dagger_{i,\alpha}c_{j,\alpha} - \mu\sum_{i,\alpha} c^\dagger_{i,\alpha}c_{i,\alpha}}_{H^0} + \underbrace{\sum_{i,j}\left(d_{ji}c^\dagger_{j\sigma}c^\dagger_{i-\sigma} + h.c.\right)}_{H^\Delta} \tag{B.1}$$

The Fourier transform can be performed using the well-known expansions,

$$c^\dagger_{i\sigma} = \frac{1}{\sqrt{V}}\sum_{\mathbf{k}} e^{i\mathbf{k}r_i}c^\dagger_{\mathbf{k}\sigma}$$
$$c_{i\sigma} = \frac{1}{\sqrt{V}}\sum_{\mathbf{k}} e^{-i\mathbf{k}r_i}c_{\mathbf{k}\sigma}$$

Separating the Hamiltonian as indicated in Eq. B.1, we get

$$\begin{aligned}
H^0 &= -t\sum_{i,j,\sigma} c^\dagger_{i\sigma}c_{j\sigma} - \mu\sum_{i,\sigma} c^\dagger_{i\sigma}c_{i\sigma} \\
&= -\frac{t}{V}\sum_{i,j,\sigma}\sum_{\mathbf{k},\tilde{\mathbf{k}}} e^{i\mathbf{k}r_i}e^{-i\tilde{\mathbf{k}}r_j}c^\dagger_{\mathbf{k}\sigma}c_{\tilde{\mathbf{k}}\sigma} - \frac{\mu}{V}\sum_{i,\sigma}\sum_{\mathbf{k}\tilde{\mathbf{k}}} e^{i\mathbf{k}r_i}e^{-i\tilde{\mathbf{k}}r_i}c^\dagger_{\mathbf{k}\sigma}c_{\tilde{\mathbf{k}}\sigma}
\end{aligned}$$

Applying the NN restriction and setting the lattice spacing to 1 leads to,

$$\begin{aligned}
H^0 &= -\frac{t}{V}\sum_{i,\sigma}\sum_{\mathbf{k},\tilde{\mathbf{k}}}\left(e^{i\mathbf{k}r_i - i\tilde{\mathbf{k}}(r_i+\hat{x})} + e^{i\mathbf{k}r_i - i\tilde{\mathbf{k}}(r_i-\hat{x})} + e^{i\mathbf{k}r_i - i\tilde{\mathbf{k}}(r_i+\hat{y})} + e^{i\mathbf{k}r_i - i\tilde{\mathbf{k}}(r_i-\hat{y})}\right)c^\dagger_{\mathbf{k}\sigma}c_{\tilde{\mathbf{k}}\sigma} \\
&\quad - \frac{\mu}{V}\sum_{i,\sigma}\sum_{\mathbf{k},\tilde{\mathbf{k}}} e^{i(\mathbf{k}-\tilde{\mathbf{k}})r_i}c^\dagger_{\mathbf{k}\sigma}c_{\tilde{\mathbf{k}}\sigma} \\
&= -\frac{t}{V}\sum_{i,\sigma}\sum_{\mathbf{k},\tilde{\mathbf{k}}}(e^{-ik_x} + e^{ik_x} + e^{-ik_y} + e^{ik_y})e^{i(\mathbf{k}-\tilde{\mathbf{k}})r_i}c^\dagger_{\mathbf{k}\sigma}c_{\tilde{\mathbf{k}}\sigma} - \frac{\mu}{V}\sum_{i,\sigma}\sum_{\mathbf{k},\tilde{\mathbf{k}}} e^{i(\mathbf{k}-\tilde{\mathbf{k}})r_i}c^\dagger_{\mathbf{k}\sigma}c_{\tilde{\mathbf{k}}\sigma} \\
&= -\frac{t}{V}\sum_{i,\sigma}\sum_{\mathbf{k},\tilde{\mathbf{k}}}(e^{-ik_x} + e^{ik_x} + e^{-ik_y} + e^{ik_y})\delta_{\mathbf{k}\tilde{\mathbf{k}}}c^\dagger_{\mathbf{k}\sigma}c_{\tilde{\mathbf{k}}\sigma} - \frac{\mu}{V}\sum_{i,\sigma}\sum_{\mathbf{k},\tilde{\mathbf{k}}}\delta_{\mathbf{k}\tilde{\mathbf{k}}}c^\dagger_{\mathbf{k}\sigma}c_{\tilde{\mathbf{k}}\sigma} \\
&= -\frac{t}{V}\sum_{i,\sigma}\sum_{\mathbf{k}}(e^{-ik_x} + e^{ik_x} + e^{-ik_y} + e^{ik_y})c^\dagger_{\mathbf{k}\sigma}c_{\mathbf{k}\sigma} - \frac{\mu}{V}\sum_{i,\sigma}\sum_{\mathbf{k}} c^\dagger_{\mathbf{k}\sigma}c_{\mathbf{k}\sigma} \\
&= -t\sum_{\mathbf{k},\sigma}(2\cos(k_x) + 2\cos(k_y))c^\dagger_{\mathbf{k}\sigma}c_{\mathbf{k}\sigma} - \mu\sum_{\mathbf{k},\sigma} c^\dagger_{\mathbf{k}\sigma}c_{\mathbf{k}\sigma}
\end{aligned}$$

Yielding the usual hopping term of the Hamiltonian

$$H^0 = \sum_{\mathbf{k},\sigma}(\varepsilon_{\mathbf{k}} - \mu)c^\dagger_{\mathbf{k}\sigma}c_{\mathbf{k}\sigma}, \tag{B.2}$$

where $\varepsilon_{\mathbf{k}} = -2t(\cos(k_x) + \cos(k_y))$. Turning the attention to the second part of Eq. B.1, we get

$$\begin{aligned}
H^\Delta &= \sum_{i,j}\left(d_{ji}c^\dagger_{j\sigma}c^\dagger_{i-\sigma} + d^\dagger_{ji}c_{i-\sigma}c_{j\sigma}\right) \\
&= \frac{1}{V}\sum_{i,j}\sum_{\mathbf{k},\tilde{\mathbf{k}}}\left(d_{ji}e^{i\mathbf{k}r_j}e^{i\tilde{\mathbf{k}}r_i}c^\dagger_{\mathbf{k}\sigma}c^\dagger_{\tilde{\mathbf{k}}-\sigma} + d^\dagger_{ji}e^{-i\mathbf{k}r_i}e^{-i\tilde{\mathbf{k}}r_j}c_{\mathbf{k}-\sigma}c_{\tilde{\mathbf{k}}\sigma}\right)
\end{aligned}$$

To implement the restriction to NN interaction and force the system to exhibit chiral p-wave superconductivity of type $p_x + ip_y$, we set

$$d_{ji} = \begin{cases} -id & , \text{ for } i = j + \hat{x} \\ id & , \text{ for } i = j - \hat{x} \\ d & , \text{ for } i = j + \hat{y} \\ -d & , \text{ for } i = j - \hat{y} \\ 0 & , \text{ otherwise} \end{cases} \tag{B.3}$$

Furthermore we have that $d_{ji}^\dagger = d_{ji}^*$. This can be seen explicitly by hermitian conjugating the Hamiltonian in Eq. B.1 and using that $H^\dagger = H$, that is the coefficients in front of $c_{j\sigma}^\dagger c_{i-\sigma}^\dagger$ ($c_{i-\sigma} c_{j\sigma}$) must be identical after the conjugation.

These definitions leads to,

$$\begin{aligned}
H^\Delta &= \frac{1}{V} \sum_{\mathbf{k},\tilde{\mathbf{k}}} \sum_j d \left(-ie^{ik_x} + ie^{-ik_x} + e^{ik_y} - e^{-ik_y} \right) e^{i(\mathbf{k}+\tilde{\mathbf{k}})r_j} c_{\mathbf{k}\sigma}^\dagger c_{\tilde{\mathbf{k}}-\sigma}^\dagger \\
&+ \left(ie^{-ik_x} - ie^{ik_x} + e^{-ik_y} - e^{-ik_y} \right) e^{-i(\mathbf{k}+\tilde{\mathbf{k}})r_j} c_{\mathbf{k}-\sigma} c_{\tilde{\mathbf{k}}\sigma} \\
&= \frac{1}{V} \sum_{\mathbf{k},j} d \left(-ie^{ik_x} + ie^{-ik_x} + e^{ik_y} - e^{ik_y} \right) \delta_{-\mathbf{k}\tilde{\mathbf{k}}} c_{\mathbf{k}\sigma}^\dagger c_{\tilde{\mathbf{k}}-\sigma}^\dagger \\
&+ \left(ie^{-ik_x} - ie^{ik_x} + e^{-ik_y} - e^{ik_y} \right) \delta_{-\mathbf{k}\tilde{\mathbf{k}}} c_{\mathbf{k}-\sigma} c_{\tilde{\mathbf{k}}\sigma} \\
&= \sum_{\mathbf{k}} d \left(\left(-2i^2 \sin(k_x) + 2i \sin(k_y) \right) c_{\mathbf{k}\sigma}^\dagger c_{-\mathbf{k}-\sigma}^\dagger + \left(-2i^2 \sin(k_x) - 2i \sin(k_y) \right) c_{-\mathbf{k}-\sigma} c_{\mathbf{k}\sigma} \right) \\
&= \sum_{\mathbf{k}} 2d \left(\left(\sin(k_x) + i \sin(k_y) \right) c_{\mathbf{k}\sigma}^\dagger c_{-\mathbf{k}-\sigma}^\dagger + \left(\sin(k_x) - i \sin(k_y) \right) c_{-\mathbf{k}-\sigma} c_{\mathbf{k}\sigma} \right),
\end{aligned}$$

This combined with Eq. B.2 yields the final Hamiltonian in $\mathbf{k}$-space,

$$H = \sum_{\mathbf{k},\sigma} (\varepsilon_{\mathbf{k}} - \mu) c_{\mathbf{k}\sigma}^\dagger c_{\mathbf{k}\sigma} + \sum_{\mathbf{k}} \left(d_{\mathbf{k}} c_{\mathbf{k}\sigma}^\dagger c_{-\mathbf{k}-\sigma}^\dagger + h.c. \right), \tag{B.4}$$

with $d_{\mathbf{k}} = 2d \left(\sin(k_x) + i \sin(k_y) \right)$ and as before $\varepsilon_{\mathbf{k}} = -2t(\cos(k_x) + \cos(k_y))$. Rewriting this to matrix form yields,

$$H = \sum_{\mathbf{k}} \begin{pmatrix} c_{\mathbf{k}\sigma}^\dagger \\ c_{-\mathbf{k}-\sigma} \end{pmatrix} \begin{pmatrix} \varepsilon_{\mathbf{k}} - \mu & d_{\mathbf{k}} \\ d_{\mathbf{k}}^* & -(\varepsilon_{-\mathbf{k}} - \mu) \end{pmatrix} \begin{pmatrix} c_{\mathbf{k}\sigma} \\ c_{-\mathbf{k}-\sigma}^\dagger \end{pmatrix} \tag{B.5}$$

Assuming the system exhibit inversion symmetry we have $\varepsilon_{\mathbf{k}} = \varepsilon_{-\mathbf{k}}$. It is now straight forward to find the excitation energies, that is the eigenvalues, which are

$$E_{\mathbf{k}} = \pm \sqrt{(\varepsilon_{\mathbf{k}} - \mu)^2 + |d_{\mathbf{k}}|^2} \tag{B.6}$$

These values can be directly related to the numerical solutions using the quantization of $\mathbf{k}$.